

---

# Mechanical Processing in the ICE Model

Anupam Prasad Vedurmudi

---



Munich 2013



---

# **Mechanical Processing in the ICE Model**

**Anupam Prasad Vedurmudi**

---

A thesis submitted for the degree of  
Master of Science  
as part of the Elite Master Program  
Theoretical and Mathematical Physics  
at the Ludwig–Maximilians–Universität  
München

presented by  
Anupam Prasad Vedurmudi  
born April 2, 1987 in Kolkata, India

Munich, June 27, 2013

This thesis was written between July 2012 and July 2013 at the Chair of Theoretical Biophysics (T35), TU München.



First Supervisor: Prof. Dr. J. Leo van Hemmen

Second Supervisor:

# **Declaration Of Authorship**

I declare that this thesis was composed by myself and that the work contained therein is my own, except where explicitly stated otherwise in the text.

Anupam Prasad Vedurmudi  
June 27, 2013

*“Oh Christ, the exhaustion of not knowing anything. Its so tiring and hard on the nerves. It really takes it out of you, not knowing anything. You’re given comedy and miss all the jokes. Every hour, you get weaker. Sometimes, I sit alone in my London flat and stare at the window, I think how dismal it is, how hard, how heavy, to watch the rain and not know why it falls.”*

– John Self  
(in Martin Amis’ *Money* (1984))

# Acknowledgements

I should and will begin by thanking my advisor Prof. Dr. J. Leo van Hemmen for introducing me to the far from uninteresting world of lizards and the clever things they do to figure out what's what and who's where. His highly contagious combination of patience and enthusiasm is something to be admired. The same can, should and will be said about Dr. Julie Goulet without whose guidance this thesis would have been around 80 pages too short. I would also like to thank Dr. Robert Helling both for organizing the TMP program and for being open to questions no matter how frequent and/or silly. Last but not the least, Mr. V., Mrs. V. and Shweta for their always unconditional and often inexplicable support.



# Contents

<b>Acknowledgements</b>	<b>vi</b>
<b>Abstract</b>	<b>xv</b>
<b>1 Introduction</b>	<b>1</b>
1.1 Mechanical Processing of Auditory Stimuli . . . . .	2
1.1.1 Evolution of Different Auditory Systems . . . . .	2
1.1.2 Pressure Difference Receiving Ears - The ICE Model . . . . .	2
1.2 Neuronal Processing of Hearing Cues . . . . .	5
1.3 Overview . . . . .	7
<b>2 The ICE Model</b>	<b>9</b>
2.1 Description of the Model . . . . .	10
2.1.1 Mouth Cavity . . . . .	10
2.1.2 Middle Ear System . . . . .	11
2.1.3 Head Model and External Sound Input . . . . .	14
2.2 Derivation of the Model . . . . .	17
2.2.1 Internal Cavity . . . . .	20
2.2.2 Vibration of the Membrane . . . . .	22
2.2.3 Vibration of Coupled Membranes . . . . .	27
2.2.4 Circuit Model . . . . .	32
<b>3 Evaluation of the Model</b>	<b>35</b>
3.1 Sound Localization Using the ICE -Model . . . . .	36
3.1.1 Membrane Vibration Velocity . . . . .	37
3.1.2 Directional Hearing Cues . . . . .	40
3.1.3 Parameter Estimation . . . . .	47
3.2 Spatial Vibration Pattern of the Membrane . . . . .	50
<b>4 Summary and Discussion</b>	<b>53</b>
4.1 Biological Relevance . . . . .	54
4.2 Open Questions . . . . .	55
<b>A Mathematica Code</b>	<b>57</b>



# List of Figures

1.1	Vertebrate Ear Evolution . . . . .	3
1.2	Cross Section of a Lizards Head . . . . .	4
1.3	EE-type coincidence detector and encoding of sound waves as membrane potentials. . . . .	6
1.4	Delay line coincidence detector - Jeffress model . . . . .	7
2.1	Illustration of a gecko's head . . . . .	9
2.2	Previous and current ICE model representations . . . . .	12
2.3	Extracolumella position on a gecko' ear. . . . .	13
2.4	Extracolumella Flection . . . . .	14
2.5	Tympanic membrane model . . . . .	15
2.6	Previous acoustic head model for geckos . . . . .	16
2.7	New acoustic head model for geckos . . . . .	17
2.8	Circular membrane eigenmodes . . . . .	25
2.9	Sectoral membrane eigenmodes . . . . .	27
2.10	Low frequency circuit analog . . . . .	33
3.1	Vibration amplitude for the common house gecko . . . . .	38
3.2	Vibration amplitude for the Tokay gecko . . . . .	38
3.3	Frequency dependence of ipsi- and contralateral membrane vibration amplitudes - common house gecko . . . . .	39
3.4	Frequency dependence of ipsi- and contralateral membrane vibration amplitudes - Tokay gecko . . . . .	39
3.5	Frequency dependence of membrane vibration amplitudes for different directions. . . . .	40
3.6	Direction dependence of membrane vibration amplitudes for different frequencies. . . . .	41
3.7	ILD plots for the common house gecko . . . . .	43
3.8	ILD plots for the Tokay gecko . . . . .	43
3.9	Direction dependence of the Internal Level Difference for different frequencies.	44
3.10	Spectral behavior of the iLDs. . . . .	45
3.11	Spectral behavior of the iTDs. . . . .	46
3.12	Variation of the iTD with direction for different frequencies. . . . .	46

3.13 Possible frequency regimes for usage of iTD and iLD cues. . . . .	47
3.14 Dependence of iTD spectrum on Quality Factor . . . . .	50
3.15 Tympanic membrane vibration profiles for the Tokay gecko. . . . .	51

# List of Tables

2.1	Functions and Parameters used in the ICE Model . . . . .	19
3.1	ICE Model geometry Parameters for the common house gecko ( <i>Hemidactylus frenatus</i> ) and the Tokay gecko. . . . .	36



# Abstract

ICE is a general model that explains the enhancement of directional hearing cues (viz. amplitude, phase difference) in animals such as lizards which have eardrums that are coupled through the mouth cavity. In this thesis we will propose a geometric model for such a system as an extension of Vossen's [13]. The model enables us to calculate the complete vibration profile of the tympanic membrane driven by the internal and external pressures. The directional cues can then be defined in terms of the phase and amplitude differences between the membrane vibrations. These cues, known respectively as the internal time and level differences (iTDS and iLDs), show a strong directionality and amplification (in terms of the input). The validity of the model is evaluated by comparing the frequency and direction dependence of these cues with membrane vibration data taken from live gekkonids. This also enables to propose possible frequency regimes for the use of iTDs and iLDs and the dependence of these regimes on system parameters. As a final step we will compare the complete vibration profile of our model tympanum with experimentally measured values.



# Chapter 1

## Introduction

Among sensory systems, the auditory system is perhaps the most ubiquitous. The development of numerous strategies for the detection and processing of auditory stimuli across several species is a testament to this fact; cf. Sec. 1.1.1. The processing of sound stimuli is fairly fast and in comparison to light stimuli, sound has two main properties - it is omnidirectional and due to its large wavelength it isn't blocked by small objects. For instance we can hear objects behind us or behind obstacles whereas the same isn't true for visual stimuli. These properties give the animal the obvious advantage of being able to react to approaching dangers that aren't yet visible. In order to fully utilize the sound stimuli, it is therefore essential that an animal is able to assess the direction or, to use the technical term, *localize* a sound source.

Before we discuss the various sound localization methods observed in nature, we first go through the fundamental steps involved in auditory perception. First, an object generates an auditory stimulus which in general can be very complex. This stimulus then propagates through a given medium (e.g. air, water) and excites the primary receiver(s) of the animal. In most terrestrial vertebrates, these take the form of *tympani* or eardrums - a pair of thin vibrating membranes which are a component of the mechanical part of the auditory system. Depending on the species, there may be an apparatus that focuses and amplifies the sound waves. In humans for example, this function performed by the external ears or pinnae. The vibrations are then transmitted by means of a set of bony or cartilaginous elements and converted into electrochemical signals that will be processed neuronally; see Sec. 1.1.

The neuronal processing system consists of building blocks called *neurons* which are connected to each other through *synapses*. The entire system is referred to as a *neuronal net* which, through a form of computation, gives rise to representations of the stimuli known as *neuronal maps*. Each neuron of the map represents a specific property, e.g. the position in space or the frequency of the stimulus and neighbouring neurons respond to similar sensory inputs. Neuronal maps serve to reconstruct stimuli as optimally as possible within the limits of processing. The precise calibration of the synapses required for stimulus reconstruction is a result of experience-based learning processes that take into account inputs from all available sensory systems.

The primary focus of this thesis is the mechanical processing that is responsible for the

sound localization ability of certain terrestrial vertebrates. Specifically, we are interested in the analytical treatment of hearing in animals that have their eardrums connected through a large mouth cavity and the enhancement of directionality in the response of such systems; see Sec. 1.1.2. Although our model can be scaled to several different species, for the purposes of a thorough comparison, we will be putting a special emphasis on lizard hearing. The questions posed by the neuronal processing of auditory stimuli in these animals although interesting, are beyond the scope of this thesis. However, in order to have a basic understanding of the neuronal basis for our analysis, we will briefly discuss the neuronal processing of the binaural cues in these animals in Sec. 1.2.

## 1.1 Mechanical Processing of Auditory Stimuli

### 1.1.1 Evolution of Different Auditory Systems

Ancestors of most modern vertebrates including frogs, turtles, lizards, birds, crocodilians and mammals developed a pair of tympani (thin vibrating membranes) to detect incoming sound waves and transmit them from the air to the ossicles in the middle ear; cf. Fig. 1.1. Despite the large variation in size and shape, two groups with fundamentally distinct constructions can be made out. Mammals possess tympani that are effectively separated from and therefore acoustically independent of each other. In contrast, the other group consisting of reptiles (lizards, turtles, crocodiles), birds and frogs have Internally Coupled Ears (for reviews see [1], [2] and [3]) wherein the tympani are connected through large Eustachian tubes as illustrated in 1.2. The evolutionary appearance of independent and coupled ears (Fig. 1.1) suggests that the latter are probably early tympanic ears.

### 1.1.2 Pressure Difference Receiving Ears - The ICE Model

The ability of humans and most other mammals to localize sources of sound depends on two kinds of information: the direction and frequency of the source may cause differences between the amplitudes (ILDs - Interaural Level Differences) and arrival times ((ITD - Interaural Time Differences) of sounds reaching both ears. These pieces of information are referred to binaural hearing cues or simply hearing cues. In mammals there is an additional source of directionality due to the shape of the pinnae which affects the spectra of sounds reaching the ear (monoaural cues). In effect, the ears are independently activated by sound pressures on their external surface. In humans, at frequencies above 1.5kHz, the amplitude differences between the eardrums are sufficient to localize the source whereas at lower frequencies the time cues are mainly used. The amplitude cues are a result of the ear farther from the source being in the 'sound shadow' of the head due to diffraction effects. The time cues are a result of the sound having to travel different paths to reach either ear and is in general not as strongly affected by diffraction.

However, most hearing animals are lack monoaural cues and the binaural cues are at best too small to affect the neural responses of the ears, [5]. These animals are in

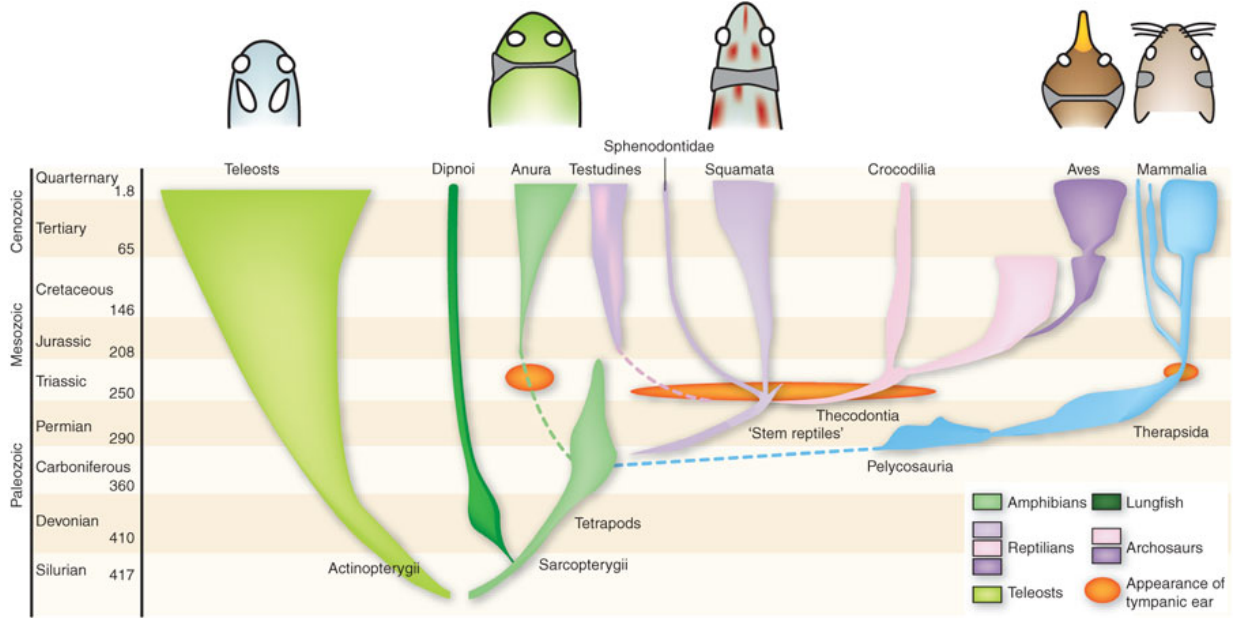


*Figure 1.1: Evolution of vertebrate ears. Tympanic middle capable of receiving airborne sound evolved independently among the ancestors of modern frogs, turtles, lizards, birds, crocodilians and mammals. Diagrams at the top show cross-sections through different heads of these animals (middle ears - gray fill). Among these middle-ear systems two distinct groups can be observed - the anura (frogs and toads), squamata (lizards and snakes) and aves (birds) form one group with ears connected through differently shaped cavities and mammals with independent ears. Figure due to Schnupp and Carr [3].*

general too small in comparison to the wavelength of sound in their typical hearing range to cause an appreciable amplitude differences due to diffraction. Nevertheless, the eardrum vibration amplitude has been found to vary strongly with direction. In order to resolve this apparent paradox it was suggested by Autrum [6] that in locusts the directionality could be a result of the ears vibrating due to the differences between the pressure on the inner and outer surfaces (see [7] for a review). The properties of such systems were also found to be analogous with the inherently directional nature of pressure gradient receivers studied by Harry Olson ([8]). Pressure difference reception has become the standard explanation for directionality in almost all small animals; the one exception being mechanically coupled eardrums in some parasitic flies, (see Robert *et al* [9]).

The pathway for sound to the inner surface of the eardrum varies. In many animals the air spaces behind the eardrums are connected by sizable air-filled passage which results in a coupling between the eardrums. This has been shown for insects ([10]), frogs ([11]) and reptiles ([4]). The sound wave may alternatively reach the inner surface of the eardrum through a different route (like the tracheal tube in crickets). Our focus is on the construction and mathematical analysis of a model for the former type of animals, i.e. animals that have their eardrums coupled through an air-filled cavity. The ICE model seeks to explain the emergence of enhanced directional cues in animals that are small relative to wavelengths in their entire hearing range. As a result, they are forced to exploit the small

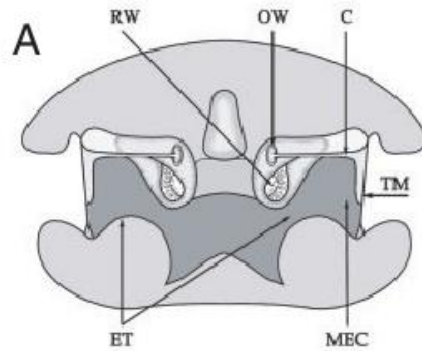


*Figure 1.2: Diagram of the cross-section of a lizards head (sceloporus). The Tympanic Membranes (TM) as well as the air inside the Middle Ear Cavity (MEC) and Eustachian Tubes (ET) are excited by incoming sound waves. Due to the considerable width of the Eustachian Tubes (ET), the air inside the Pharynx (P) is excited as well. The vibration of the tympanum causes a movement of the attached middle ear, Columella (C) whose lever construction transmits the vibrations to the Oval Window (OW), the membrane at the entrance of the fluid filled cochlea. Figure taken from [4]. The vibration of the OW excites the fluid in the Cochlea which gives rise to a frequency-dependent activation of the embedded basilar membrane and underlying auditory nerve fibers. The Round Window (RW) is a membrane at the end of the cochlea that serves to compensate the pressure within the fluid.*

time differences between the inputs between their ears to localize a sound source. Using these small ITDs, the system generates amplified time differences (which we will refer to as iTDs - Internal Time Differences) and direction dependent amplitude differences (which we will refer to as iLDs - Internal Level Differences) between the tympani.

The primary advantage of pressure difference receiving ears is to compensate for a small body size relative to sound wavelengths. It has however also been suggested that there is another reason for this adaptation. The natural habitats of such animals is usually close to the ground resulting in a severe degradation of directional cues due to the presence of obstacles. Amplitude cues are especially affected due to multiple reflections and other deviations from a free sound field. In contrast, the contribution to the scatter of phase cues due to diffraction are not nearly as dramatic (the degradation of these cues for a grasshopper in its natural grassland habitat was studied my Michelsen and Rohrseitz [12]). Therefore, by only exploiting phase cues, these animals would have a much more accurate localization strategy than by exploiting amplitude cues. Moreover, the scattering of both amplitude and phase in dense habitats increases with frequency suggesting that animals in these habitats should prefer to use rather low frequencies for communication.

Following Vossen [13], we refer to our model as “ICE” (Internally Coupled Ears). Our goal is to analyse the physics behind the production of the enhanced differences (iTД/iLD). In particular we are interested in the frequency and direction dependence of the hearing cues. The problem of directional hearing in lizards was previously treated by Vossen (see Chapter 2 of [14] and Vossen *et al* [13]). Here, an analytical model of internally coupled ears with a cylindrical air cavity was first presented. This thesis aims to be an extension of the previous work wherein we seek to provide an analytical model that reflects the

frequency and directional behaviour of such systems in nature. Our work deviates in the treatment of the following aspects -

- While constructing the mouth cavity we place an emphasis on maintaining its volume resulting in different radii for the tympanum and the cylindrical cavity; See Sec. 2.1.1.
- For the pressure inside the cavity (See Sec. 2.2.1) we propose a different set of modes that represent it more accurately.
- The treatment of the membrane and its transducer - the extracolumella (See Sec. 2.1.2). We propose a construction that is easier to treat analytically and reproduces the vibration patterns fairly well.

## 1.2 Neuronal Processing of Hearing Cues

The neuronal processing of auditory signals starts after the tympanic vibrations are transmitted by the columella (the middle ear bone that is attached to the tympanum) to the oval window, a membrane at the entrance of the cochlea; see Fig. 1.2. The vibration of the oval window results in the vibration of the fluid within the cochlea and of the embedded basilar membrane. The basilar membrane has a systematically varying stiffness resulting in each of its parts reacting to a specific frequency. Auditory nerve fibres that respond to a small range of frequencies do so by being enervated by the movement of specific regions of the basilar membrane. In this manner, the basilar membrane functions to decompose sound frequencies.

Early stages of auditory pathways in birds and mammals contain synaptic relays designed to preserve the temporal fine structure of acoustic stimuli with great accuracy. Studies of neural processing in Tokay geckos have also shown similar properties [15]. These animals possess cochlear nuclei (the collections of neurons that receive input from the cochlear nerve) that are specialized either for the computation of time differences (iTd/ITD) or level differences (iLd/ILD) between the tympani. The neurons sensitive to level difference are excited by the input from one ear and inhibited by the other. These neurons are for obvious reasons known as 'EI' neurons and respond most strongly when the sounds come from the excitatory ear. The inhibitory ear, on the other hand sits on the far side of the head resulting in an increased firing rate of the neurons due to reduced inhibition. Similarly, as the sound source moves closer to the inhibitory ear, the neural firing rates decline due to increased inhibition. Thus, the neural firing rate encodes the sound source position.

In contrast, the neurons sensitive to time differences are excited by inputs from both ears ('EE' neurons, Fig. 1.3a). The strength of the excitation depends on the exact relative timing of the inputs. Just as is the case for larger animals, the level differences are more pronounced and most effective at higher frequencies and the time difference cues at lower frequencies. Sound waves are encoded by neurons as sinusoidal membrane potentials. The primary sensory neurons, known as afferent neurons, phase lock to the input stimulus and are most likely to fire near the peak of the sound wave. Their synaptic potentials (formed

due to differences in ion concentration) sum to produce fluctuating membrane potentials which resemble the stimulus waveform; see Fig. 1.3b.

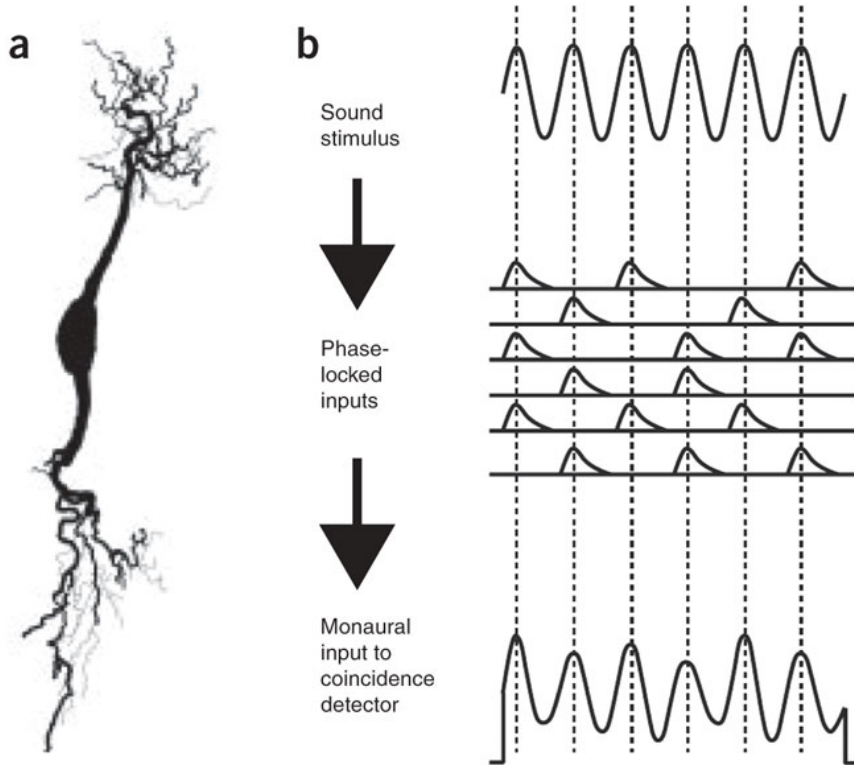


*Figure 1.3: (a) Anatomy of an 'EE-type' coincidence detector neuron. Sound signals from both ears converge through the two prominent dendrites (the hair like extensions on either end). (a) Encoding of sound waves as sinusoidal membrane potentials. Nerve fibers phase lock to the sound stimulus and are therefore most likely to fire near the peaks. Their excitatory synaptic potentials sum to produce membrane potentials which resemble the stimulus waveform. Figure taken from [3].*

The neurons responsible for the processing of time difference queues were classically thought to be organized in a 'delay line and coincidence detector' arrangement, commonly known as the 'Jeffress model'[16]. According to this model, the firing of individual neurons is response to precisely synchronized excitation from both ears, and systematically varied axonal conduction delays along the length of the nucleus serve to offset ITDs. Thus each neuron is tuned to a specific time delay value that cancels the signal delay from the left and right ear; see Fig. 1.4. The appeal of the Jeffress model lies in the elegant way it converts systematic variations in the iTD/ITD into a topographic map of the sound source location. Initial experimental evidence from birds ([17], [18]) provides strong support for the existence of such a delay line arrangement.

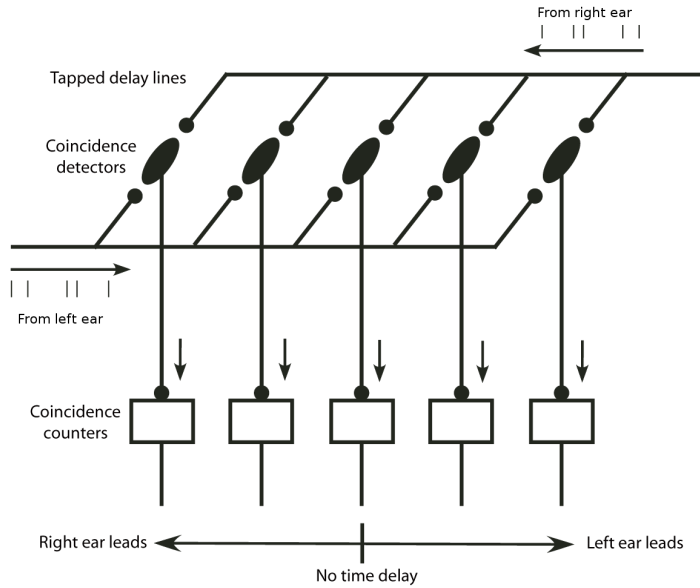


*Figure 1.4: A very simplified schematic representation of the Jeffress model. The coincidence detector neurons ('EE-type') simultaneously receive inputs from both ears through different delay lines. The coincidence counters fire when the inputs to the detectors are synchronized. For example when a sound reaches the left ear first, the inputs reaching the rightmost detectors are more synchronized due to the signal from the left ear being delayed.*

## 1.3 Overview

Our study will take place in two main steps. In Chapter 2 we will present our model for the mechanical processing of auditory signals in systems with internally coupled ears - the ICE Model. Since our focus is on an analytical model, we would like to have a system that reduces to tractable mathematical expressions so that we can clearly see the dependence of the system's behaviour on its parameters. To this end we will model the combination of the Eustachian tubes, middle ear cavity and pharynx as a single continuous cylindrically shaped air cavity; see Sec. 2.1.1. The ears will be modelled as linear elastic membranes that are circular with an omitted sector replaced by a non-moving plate that corresponds to the extracolumella - the extension of the columella that is in contact with the ear. The sound inputs to both the ears will be modelled as pressure waves of a given frequency with a phase difference corresponding to the azimuth of the object that depends on the head size and frequency. The aim of the chapter is to find expressions for the quantities which give us the directional output of the system.

In Chapter 3 will evaluate the validity of our model by comparing the calculated values of the membrane vibration velocity with experimentally determined quantities; see 3.1.1. In addition to testing the directional frequency response of the system we will also define quantities that could serve as directional cues. These two quantities are known as the iTD (*Internal Time Difference*) which measures the delay between the membrane vibrations and the iLD (*Internal Level Difference*) which measures the difference in their vibration

amplitudes; Sec. 3.1.2. These quantities are defined in contrast to the *Interaural* Time and Level Differences which serve as directional cues in the absence of coupling. Due to the difficulty of measurement of certain membrane properties (e.g. fundamental frequency, damping coefficients), in Sec. 3.1.3 we will also provide means of estimating these quantities from observations. In the final section of this chapter, Sec. 3.2, we will compare the vibration profile of our model tympanum with that of a realistic tympanum and thereby seek to explain the complex patterns of the observed.

# Chapter 2

## The ICE Model

Several terrestrial vertebrates, e.g. lizards, frogs, alligators and many birds, possess a hearing mechanism very different to that of mammals: their tympanic membranes are coupled through large Eustachian tubes and a large mouth cavity resulting in the influence of the vibrations of one tympanic membrane on those of the other. This is illustrated in 2.1. The typically small head sizes (compared to sound wavelength) of these animals result in small phase differences (ITDs) and negligible amplitude difference (ILDs) between the ears. The coupling serves to enhance the ITDs and create level differences between the tympanic vibrations. These differences show directionality and serve as hearing cues for localization.

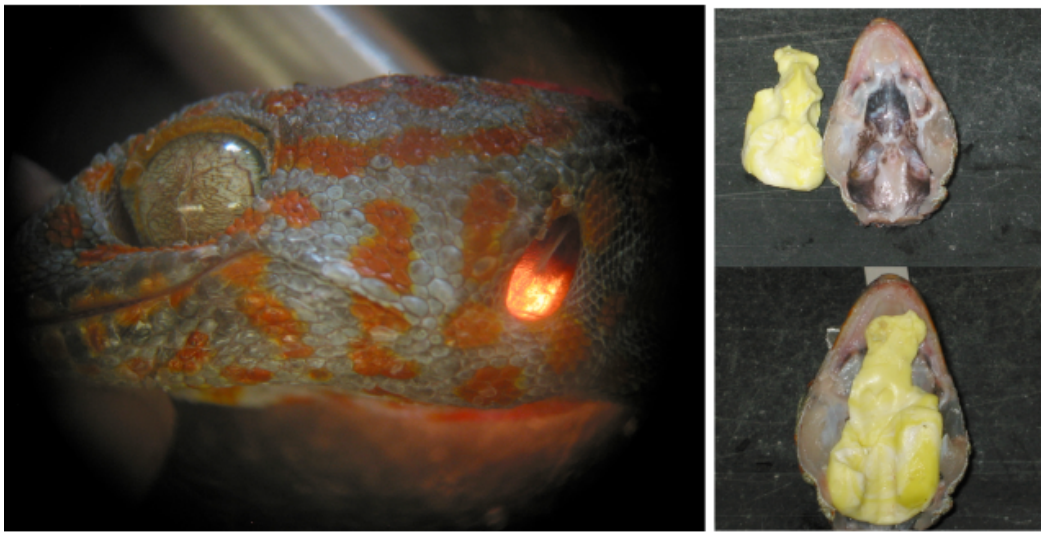


Figure 2.1: Left: Picture of a Tokay gecko's head with the snout pointing to the left. The tympanic membrane is illuminated from behind by a light source on the other side of the head. The cartilaginous extracolumella can be seen attached to the upper part of the membrane. Right: Cast imprint of the mouth cavity of the gecko with the snout pointing to the top. The figures illustrate the coupling of the tympani through the mouth cavity. Photographs courtesy of Jakob Christensen-Dalsgaard.

Proceeding from the earlier work done by Vossen [14] and Vossen *et al* [13], in this

chapter we present a model for such a system of coupled ears with an emphasis on lizard hearing - specifically the Tokay gecko and the common house gecko. Our goal is to demonstrate its main aspect of such a system - the coupling of the eardrums through the mouth cavity. The main components of such a system are the mouth-cavity, the two tympani and the two *extracolumella* (one on each tympanum). In general, the shape of the mouth-cavity is highly irregular and therefore not conducive to an analytical treatment. Moreover, the system corresponds to a pair of coupled second-order PDE's with moving boundaries. For this reason we will need to make further approximations in order to facilitate an analytic solution.

In order to make the system more analytically tractable we will, as before, study a geometry in which a pair of rigidly clamped linear elastic membranes are coupled through a cylindrical cavity. The cylindrical geometry allows an accurate calculation of the pressure distribution inside the cavity at both low and high frequencies. By accounting for the presence of the asymmetrically attached extracolumella, we will also explain the complex vibration patterns of the membrane. We will conclude this chapter with a comparison of our model with previous methods that have used a electrical circuit analogy to model the system. At the end of this chapter, we will have the expressions that describe the steady-state vibrations of both eardrums as a function pressure amplitude, direction and frequency.

## 2.1 Description of the Model

Before heading to a quantitative analysis of the ICE model, we will first need to list its basic components. and justify their properties based on realistic anatomical properties of the vertebrates in question. Our emphasis is on an analytical treatment of the ICE model. In Sec. 2.1.1, we will describe the cylindrical model for the mouth cavity and state the reasons for our choice of the geometry and the dimensions used. We will then proceed to describe the middle ear system and its main components of interest, the *extracolumella* and the *tympani* in Sec. 2.1.2. Finally, in Sec. 2.1.3 we will analyze the dependence of the acoustic input to both eardrums on the direction of the sound source, head size and shape.

### 2.1.1 Mouth Cavity

In the earlier treatment of the ICE model, the mouth cavity is modelled as a simple cylinder closed at both ends by rigidly clamped (baffled) circular membranes; these model the tympanic membranes. As shown by Vossen in [14, p. 21] and [13], the length of the cylinder was chosen to be equal to the interaural distance and the radius of the model tympanum is determined from the typical area of the realistic tympanum. The advantage of using a cylindrical cavity model for the mouth cavity is that the pressure distribution inside the cavity is easy to calculate. The pressure distribution inside the cavity becomes highly

non-uniform with increasing frequency and a cylindrical cavity simplifies its calculation<sup>1</sup>.

On the other hand, in this description the small area of the tympani results in a cavity volume which is an order of magnitude smaller than that of the realistic mouth-cavity in the corresponding animal. In general, a smaller volume results in a stronger coupling between the tympani. The exact nature of this coupling will be discussed in the next chapter when we perform a thorough evaluation of the complete system.

In order to get around this problem we make some slight modifications to the model. Essentially, we maintain the cylindrical shape of the internal cavity but require it to have a volume which is equal to that of the realistic cavities in typical specimens. This volume is denoted by  $V_{\text{cav}}$ . While maintaining the same tympanum size and interaural distance we can therefore calculate the radius of the cylinder as,

$$a_{\text{cyl}} = \sqrt{\frac{V_{\text{cav}}}{\pi L}} \quad (2.1)$$

where  $a_{\text{cyl}}$  is the cylinder radius and  $L$  is the interaural distance. Simply put, the model consists of a cylindrical shell of radius  $a_{\text{cyl}}$  and length  $L$  with circular holes on either side with the radius of the tympanic membrane,  $a_{\text{tymp}}$ . These holes are in turn closed by rigidly clamped membranes which will be described in the next section. The previous and current geometric representations of our model are shown in figures 2.2a and 2.2b. The darkly shaded circular surfaces in fig. 2.2b at ends 0 and  $L$  correspond to the two eardrums.

We will be working with the cylindrical polar coordinates,  $(r, \phi, x)$ . The direction along the cylindrical axis is denoted by  $x$  and  $(r, \phi)$  are the polar coordinates of the plane perpendicular to the  $x$ -direction. Directions outward from the cylinder are taken as positive (in  $x$ ) and those inward are taken as negative.

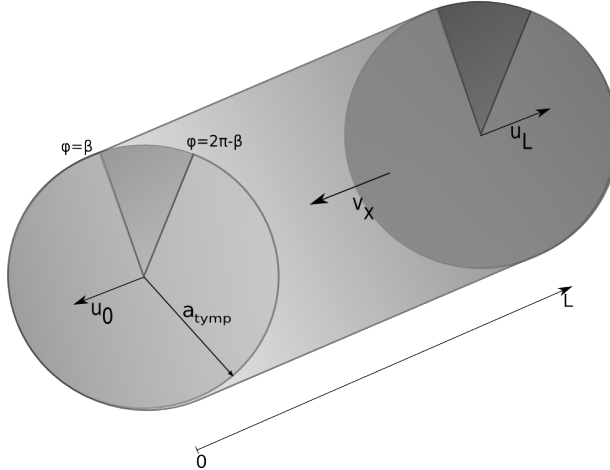
### 2.1.2 Middle Ear System

The main components of the middle-ear of lizards are the two eardrums, the columella and the two cartilaginous extracolumella. The tympanic membrane or the eardrum is a thin membrane that separates the outer ear and the middle ear and vibrates in response to external sound waves. Unlike humans, lizards possess only a single middle ear bone, the *columella*, that is connected to both eardrums by means of a cartilaginous element, the *extracolumella*. The placement of the extracolumella can be made out at the top of the eardrum in Fig. 2.3.

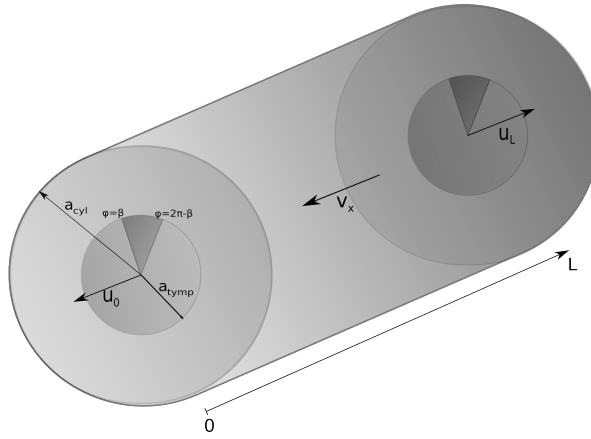
The membrane-extracolumella-columella system functions as a second-order lever where the membrane - driven by the internal and external pressures - causes a displacement of the extension of the extracolumella (known as the inferior process). This motion is in turn transmitted via the columella and columellar footplate to the inner ear (cochlea). The inner-ear translates this motion into electrochemical impulses which will be passed on

---

<sup>1</sup>We are in effect modelling the combination of the middle ear cavity, pharynx and Eustachian tubes as a single continuous cavity. This is a reasonable approximation due to wide Eustachian tubes typically seen in lizards.



(a) The previous geometric representation of the ICE model.



(b) The representation of the new model.

Figure 2.2: The bold arrows represent the direction conventions along the cylinder's axis. The new model is represented by a cylinder of radius  $a_{cyl}$  and length  $L$  closed at both ends by sectoral membrane of radius  $a_{tymp}$ . The darkly shaded region corresponds to the extracolumella; see Sec. 2.1.2.

to the brain via the auditory nerve; cf. Fig. 1.2. The columella-extracolumella system effectively transmits the mechanical vibrations from the eardrums to the inner ear. In the human middle-ear, the same function is performed by the bones *malleus*, *incus* and *stapes*, which are collectively known as the ossicles.

For low frequencies (below 4kHz), the extracolumella (or more accurately, the inferior process of the extracolumella) moves as a completely stiff bar. It was shown by Manley [19] that the extracolumella begins to flex at higher frequencies - this is illustrated in fig. 2.4. This is partly responsible for the poor high-frequency response of gecko middle ears - a feature also observed in other non-mammalian vertebrates. The reason for this is that, due to the flection some energy is lost and not transferred to the columella.



*Figure 2.3: Close up shot of a Tokay gecko's tympanum. In this figure the scale and shape of a typical Tokay gecko tympanum is illustrated. Also apparent is the position, size and shape of the extracolumella on the left part eardrum can be discerned clearly (inside the red box). Its asymmetrical placement on the tympanum surface can also be made out. In our analysis we approximate the ellipsoid membrane by a circular one of the same area. Photograph courtesy of Yezhong Tang.*

### Tympanic Membrane

The extracolumella applies a significant mechanical load on the tympanum and thereby precludes its treatment as a freely vibrating membrane. Furthermore, the contact surface of the malleus on the human eardrum is more or less symmetric whereas the extracolumella is attached asymmetrically. This has important physical consequences - especially in the observed vibration patterns of the membrane.

In the previous treatment of the ICE model, the tympanum was modelled as a clamped circular membrane with asymmetrically attached sectoral load between  $-\beta < \phi < \beta$  ([13]). This manifests itself as an additional boundary condition at  $\phi = \beta$  and  $\phi = -\beta$  which has to be satisfied via a numerical approximation. While this method has the advantage of being able to accurately reproduce the complex vibration patterns of the eardrum, it does not lend itself well to an analytical treatment of the coupled system.

In our study, we will follow a slightly different path. The tympanic membrane will be modelled as a rigidly clamped sectoral membrane. This means that in addition to the radial boundary at  $a_{\text{tym}}^r$ , we have a new set of boundaries at  $\phi = \beta$  and  $\phi = 2\pi - \beta$  where the membrane vibration is set to zero. This is illustrated in 2.5. The membrane material will be assumed to be linear-elastic. As before, the equations describing the vibrations of the membrane will consequently be linear 2<sup>nd</sup>-order PDE's.

In our model for the tympanic membrane-extracolumella system we have modelled

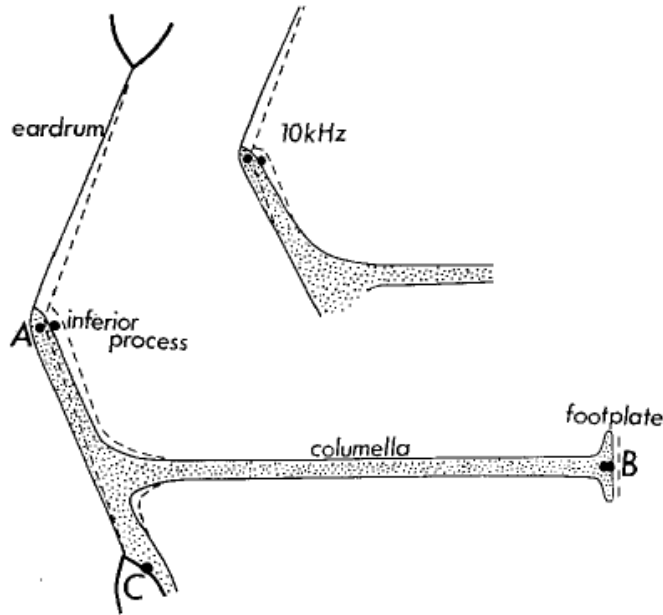


*Figure 2.4: Operation of the middle ear lever in geckos reproduced from [19]. The inferior process of the extracolumella (A-C) hinges at point C at low frequencies. Also shown is the flection of the inferior process of the extracolumella.*

the extracolumella as non-moving by effectively setting its mass of the extracolumella to infinity. While neglecting its motion altogether may seem counterintuitive at first, we will later see that this assumption, while simplifying the problem analytically, has little effect on the physical phenomenon of interest, viz. the coupling between the eardrums and the amplification of hearing cues. This will be discussed in-depth in Chapter 3.

### 2.1.3 Head Model and External Sound Input

In realistic environments the acoustic fields experienced by animals are often very complex. In addition to sound waves radiated directly from one or more sources in general, they also involve waves reflected from objects in their immediate neighbourhood. Higher animals such as humans possess the neural power to carry out the sophisticated signal processing needed to derive useful information from these signals. Simpler animals like geckos respond to simpler cues - usually the direct field from the nearest or strongest source.

We can therefore model our incoming wave as the simple case of an incident plane wave of a certain frequency. This input is specified in terms of its intensity, frequency and direction. Such a stimulus can be generated in an anechoic chamber from loudspeakers which are placed at a distance from the animal that is large compared to the animal's size and the wavelength of the sound involved. Such experimental-setups are more thoroughly described by Christensen-Dalsgaard and Manley ([4], [21]) and Christensen-Dalsgaard, Tang and Carr ([15]).

The amplitude of the sound pressure incident on both ears can be taken as uniform in

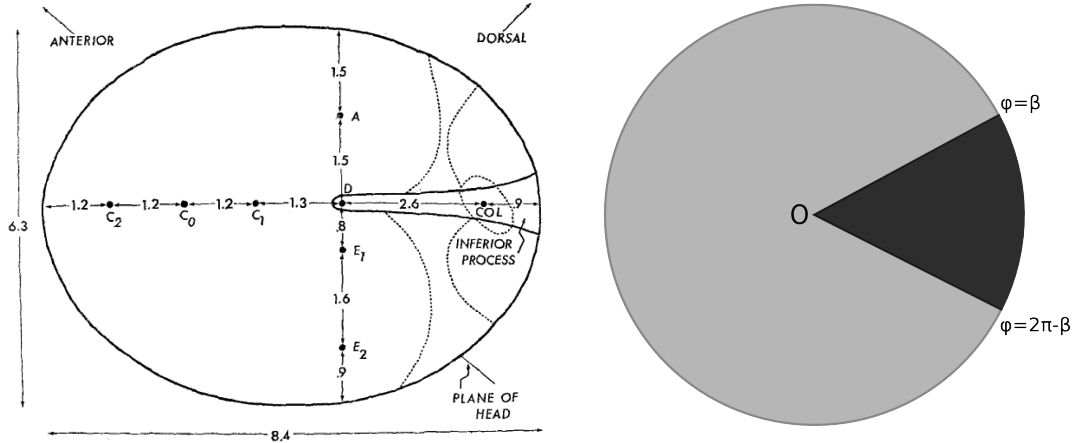


Figure 2.5: Left: Sketch of the eardrum of a Tokay gecko as seen from the outside taken from Manley, [20]. “COL” is the approximate position opposite the extracolumella insertion. The dots indicate the positions for measurements and will be discussed briefly in the next chapter. Dimensions in millimeters. Right: Our model for the loaded tympanic membrane. The lightly shaded region is modelled as a linear elastic membrane whereas the darkly shaded region ( $\beta < \phi < 2\pi - \beta$ ) represents the contact surface of the extracolumella and the membrane.  $\beta$  corresponds to the breadth of the extracolumella and is estimated from anatomical data.

over the surface of the membrane. The spatial variation can be safely neglected because the typical eardrum is less than 5mm in diameter whereas the smallest sound wavelengths in the hearing range of the larger lizards (eg. Tokay gecko) is around 70mm (4000 Hz) and is around 50mm (7000 Hz) for the smaller lizards (eg. Hemidactylus). In other experiments, a similar stimulus has also been provided by means of a headphone sealed to the ear ([22]).

In general the sound on the other side of the head will differ in phase as well as amplitude. This is a result of the diffraction of sound around the head and body of the animal. The exact variation depends on the size of the animal and the frequency of the incident wave. Due to the typically small head size of geckos, the amplitude variation (known as shadowing) is negligible ([7]). The phase difference, although small compared to those in larger animals, cannot be neglected. We can therefore consider the sound wave with angular frequency  $\omega$  to have a constant (pressure) amplitude  $p$  on the head.

In the earlier ICE model, the effect of diffraction on the phase difference was neglected as well. The phase difference is found directly from the phase difference  $\Delta$  as shown in fig. 2.6. As a result, the sound pressure inputs at both ears is given by,

$$p_0 = pe^{j\omega t} e^{j\Delta/2}, \quad p_L = pe^{j\omega t} e^{-j\Delta/2}, \quad \Delta = kL \sin \theta. \quad (2.2)$$

We note that in defining the input in this way, we've emphasized the symmetry of the system. The ear closer to the sound source is referred to as the *ipsilateral* ear the one further away from the source is referred to as the *contralateral* ear. The terms ipsi- and contralateral also refer to the stimuli meaning “the response of the ipsilateral ear” is equivalent to “the response of the ear to ipsilateral stimulus”. We have also chosen a coordinate

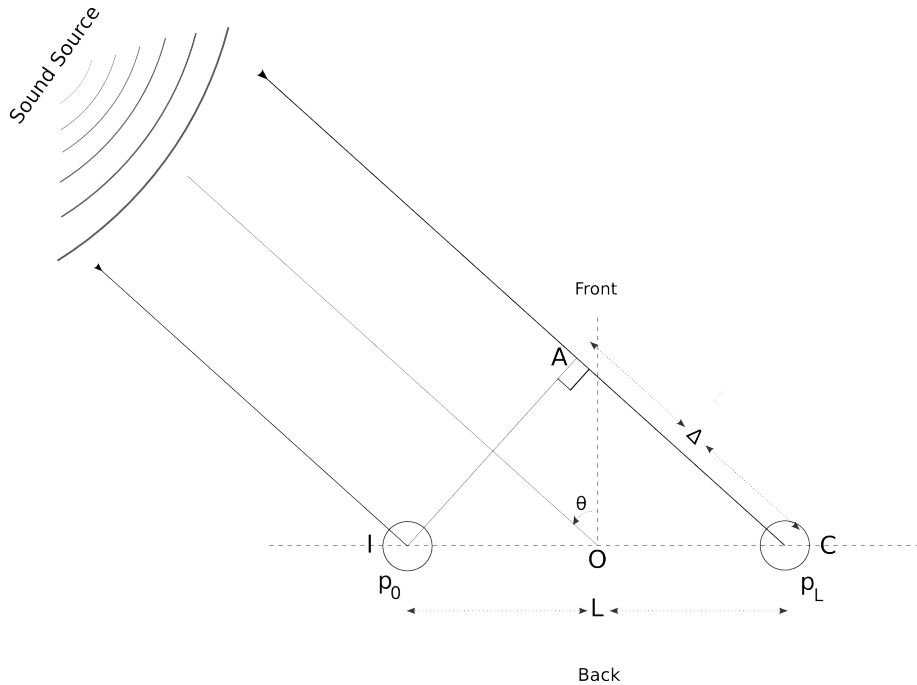


Figure 2.6: The previous acoustic head model for geckos. Depending on the angle of the sound source  $\theta$ , the distance between the sound source and the contralateral ear is longer than its distance from the ipsilateral ear. The extra distance travelled by the sound wave to reach the contralateral ear is  $L \sin \theta$  which gives rise to a phase difference  $\Delta = kL \sin \theta$ . However, this model neglects the increased phase difference due to diffraction effects which can be significant.

system relative to the *median-sagittal* plane or the head midline of the animal and  $\theta$  gives the angle of incidence of this sound wave relative to this plane. For more complex auditory systems we would require two angles  $(\theta, \phi)$  to describe the three-dimensional system but in our analysis this is unnecessary. For the animals we are concerned with, i.e. geckos, the natural predators and prey are usually present on the same plane as the animal and our assumption is therefore reasonable. According to our convention,  $\theta = 0^\circ$  corresponds to objects directly in front of the animal and  $\theta = \pm 180^\circ$  to objects directly behind. In our model we model the head as a sphere with a diameter equal to the interaural separation. As a result the sound has to travel around the head in order to reach the contralateral ear resulting in a longer path. The frequency domain solution for the diffraction of sound around a sphere was obtained by Lord Rayleigh at the end of the 19<sup>th</sup> century ([23],[24]). The expressions are greatly simplified at low frequencies and the phase difference is simply increased by a factor of 1.5. The new model is illustrated in Fig. 2.7. Therefore, the form of the input remains the same as in (2.2) except for a new phase difference  $\Delta_{new} = 1.5\Delta$ .

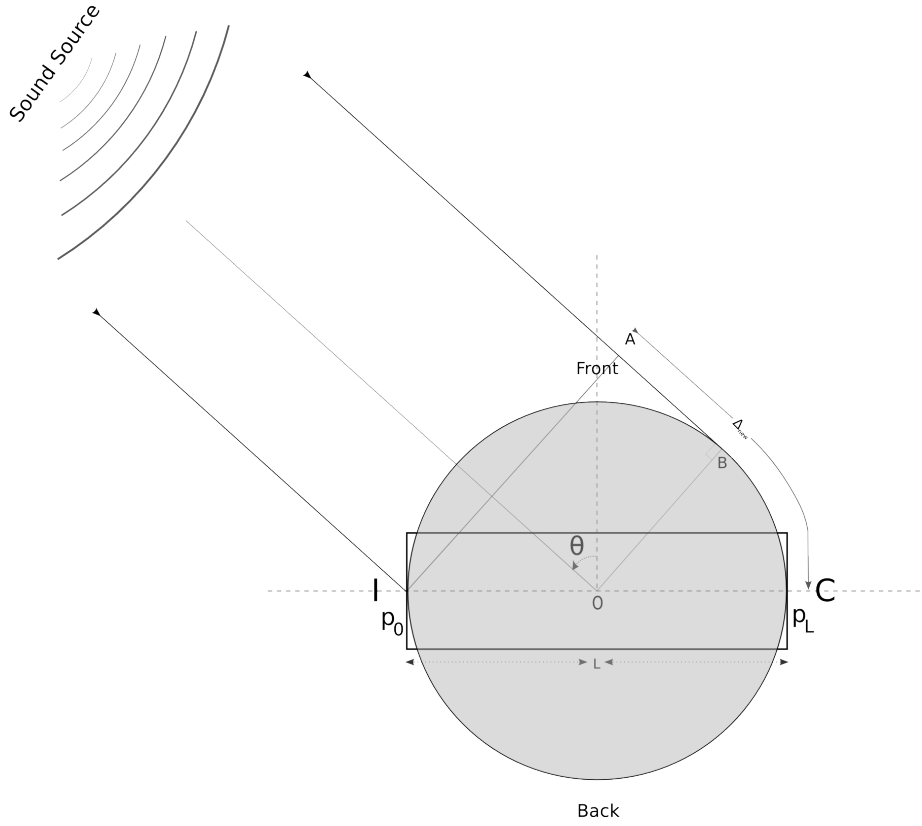


Figure 2.7: The acoustic head model for geckos. The rectangular outline is the internal cavity. As before, the sound wave has to travel an extra distance to reach the contralateral ear. In this case we have accounted for the influence of diffraction around the head on the phase difference between the inputs to both ears resulting in an increased phase difference  $\Delta_{new} = 1.5\Delta$ .

## 2.2 Derivation of the Model

We will now use the previously described physical model to derive the main expressions of interest in the ICE model - the membrane vibration profiles, the ipsi- and contraeletateral filters and the cavity pressure distribution. We will thus find an expression for the pressure distribution in the cylindrical cavity and for the membrane vibrations subject to an external stimulus. After applying the appropriate boundary conditions to relate the membrane vibrations to the internal pressure, we will find the expression for the membrane vibrations as a function of direction and frequency.

We will start in Sec. 2.2.1 by finding a general solution to a 2<sup>nd</sup>-order PDE - the 3D wave equation - that describes the pressure distribution inside the cylindrical cavity. In this section we will introduce the main boundary condition the pressure will be subject to - the “no-penetration” boundary condition. This is a physical requirement that results from the fact that the air inside the cavity does not penetrate a solid boundary.

In Sec. 2.2.2 we will solve for the vibrations of the tympanic membranes. As an example, we will find an expression for the free and periodically driven vibrations of a

circular membrane. Using the methods developed in this section, we will solve for the vibrations of a sectoral membrane - which, as we have already discussed, models the loaded tympanum. The final expression will correspond to the steady-state vibrations of a linear elastic membrane. As we neglect the transient response of the membrane, we will also discuss the circumstances under which this is justified.

Table 2.1: Functions and Parameters used in the ICE Model

$\theta$	Direction of the sound source with respect to the head midline.
$\omega$	Angular frequency of the incoming sound wave.
$k$	Wavenumber $k = \omega/c$ with $c = 343\text{m/s}$ being the speed of sound.
$p$	Pressure amplitude of the incoming sound wave.
$\Delta$	Phase difference between the sound wave reaching the contra- and ipsilateral ear.
$p_{0/L}$	Sound pressure on the ( $x = 0$ ) and ( $x = L$ ) tympani respectively.
$(x, r, \phi)$	Cylindrical polar coordinates with $x$ being the axial direction.
$L$	Interaural separation and length of cylinder.
$a_{\text{cyl}}$	Radius of cylinder.
$a_{\text{tym}}$	Radius of tympanum.
$\beta < \phi < 2\pi - \beta$	Extent of the vibrating part of the membrane. The rest of the circle corresponds to the extracolumellar footplate.
$V_{\text{cav}}$	Volume of the cavity.
$J_q$	Order $q$ Bessel function of the first kind.
$\mu_{\text{qs}}, \nu_{\text{qs}}$	Respectively - $s^{\text{th}}$ zero and $s^{\text{th}}$ extremum of the above Bessel function.
$f_{\text{qs}}(x, r, \phi)$	Orthogonal modes for the pressure distribution inside the mouth cavity.
$\zeta_{\text{qs}}$	Wavenumber of the above modes in the $x$ -direction.
$p(x, r, \phi; t)$	Pressure distribution inside the mouth cavity.
$v_x(x, r, \phi; t)$	Velocity function inside the mouth cavity.
$u_{\text{mn}}(r, \phi; t)$	Eigenmodes of the membrane displacement function.
$\omega_{\text{mn}}$	Eigenfrequency of the above eigenmodes.
$Q$	Quality factor of the membrane.
$\Psi(r, \phi; t)$	Driving pressure on the membrane.
$u_{0/L}(r, \phi; t)$	Membrane displacement function.
$C_{\text{mn}}^{0/L}$	Membrane vibration expansion coefficients.
$S^{0/L}(t)$	Total membrane displacement.
$G_{\text{ipsi}}(r, \phi)$	Ipsilateral filter.
$G_{\text{contra}}(r, \phi)$	Contralateral filter.

In Sec. 2.2.3 we will conclude by using our knowledge to solve for the vibration of the fully coupled system. In this section we will proceed by applying the velocity boundary condition at either end of the cylinder. In order to help with our analysis, we will present

a simplification scheme for this boundary condition. We will end this section by defining the ipsi- and contralateral filters. The final expressions that give us the vibrations of the tympanic membranes as a function of the external pressure with the influence of the internal cavity encoded in the ipsi- and contralateral filters. We have listed the main parameters and functions used in our analysis (including the geometry parameters) in Table 2.1.

### 2.2.1 Internal Cavity

We assume that the air inside the cavity obeys linear acoustics (cf. acoustic textbooks such as [25, p. 313] and [26, p. 247] ). This means that the air moves due to pressure  $p(x, r, \phi; t)$  whose distribution inside the cavity is given by the 3D acoustic wave-equation in cylindrical polar coordinates,

$$\frac{1}{c^2} \frac{\partial^2 p(x, r, \phi, t)}{\partial t^2} = \frac{1}{r} \frac{\partial}{\partial r} \left( r \frac{\partial p(x, r, \phi, t)}{\partial r} \right) + \frac{1}{r^2} \frac{\partial^2 p(x, r, \phi, t)}{\partial \phi^2} + \frac{\partial^2 p(x, r, \phi, t)}{\partial x^2} \quad (2.3)$$

where  $c$  is the sound propagation velocity. The complete solution must take into account the boundary conditions at and within the cavity walls and the ones at the air-membrane interface. We also note that the above equation implies that the animal's mouth is closed, which is typical for a waiting animal. In order to solve (2.3) for a particular frequency  $f$  (angular frequency  $\omega = 2\pi f$ ), we use the following separation ansatz

$$p(x, r, \phi, t) = f(x)g(r)h(\phi)e^{j\omega t} \quad (2.4)$$

which after substitution into the acoustic wave-equation leads to,

$$\begin{aligned} k^2 f(x)g(r)h(\phi) + f(x)h(\phi) \left[ \frac{\partial^2 g(r)}{\partial r^2} + \frac{1}{r} \frac{\partial g(r)}{\partial r} \right] \\ + f(x)g(r) \frac{1}{r^2} \frac{\partial h(\phi)}{\partial \phi} + \frac{\partial^2 f(x)}{\partial x^2} = 0 \end{aligned} \quad (2.5)$$

with  $k := \omega/c$ . This results in the following set of separated ODE's,

$$\frac{d^2 f(x)}{dx^2} + \zeta^2 f(x) = 0 \quad (2.6)$$

$$\frac{d^2 h(\phi)}{d\phi^2} + q^2 h(\phi) = 0 \quad (2.7)$$

$$\frac{\partial^2 g(r)}{\partial r^2} + \frac{1}{r} \frac{\partial g(r)}{\partial r} + \left[ \underbrace{(k^2 - \zeta^2)}_{=: \nu^2} - \frac{q^2}{r^2} \right] g(r) = 0 \quad (2.8)$$

with separation constants  $q$  and  $\zeta$ . The last equation is the Bessel differential equation [27, p. 313] and its general solution is given by,

$$g(r) = C_{qs} J_q(\nu r) + D_{qs} Y_q(\nu r). \quad (2.9)$$

$J_q$  and  $Y_q$  are the order- $q$  Bessel functions of the first and second kind respectively. The Bessel function of the second kind can be ignored as it diverges at  $r = 0$ . The solutions to the separated equations are therefore given by,

$$f(x) = e^{\pm\zeta x}, \quad h(\phi) = e^{\pm j\phi}, \quad \text{and} \quad g(r) = J_q(\nu r) \quad (2.10)$$

with a specific solution to (2.3) given by,

$$p(x, r, \phi; t) = [(A^+ e^{jq\phi} + A^- e^{-jq\phi}) e^{j\zeta x} + (B^+ e^{jq\phi} + B^- e^{-jq\phi}) e^{-j\zeta x}] J_q(\nu r) e^{j\omega t}. \quad (2.11)$$

The coefficients  $A^\pm$ ,  $B^\pm$ ,  $q$ ,  $\zeta$  and  $\nu$  will be subsequently determined by the boundary conditions. Before we move on to the boundary conditions we should note that in general, the time component of the pressure also has a *backward-moving* component, i.e.  $e^{-j\omega t}$ . By making the ansatz in (2.4), we have implicitly made use of the fact that the form of the input as given in (2.2) constrains the pressure to only have a *forward-moving* component, i.e.  $e^{j\omega t}$ .

## Pressure Boundary Conditions

There are three sets of boundary conditions -

- Continuity and smoothness in  $\phi$  which is equivalent to  $h(0) = h(2\pi)$  and  $h'(0) = h'(2\pi)$  where,  $h' = dh/d\phi$ .
- Vanishing of the normal derivative at the cavity walls -  $g'(a_{\text{cyl}}) = 0$  ( $a_{\text{cyl}}$  is the radius of the cylinder).
- Equating the membrane velocity to the velocity function at the membrane boundaries (to be discussed in the next section).

The first set of requirements is obvious. This reduces (2.11) to

$$p(x, r, \phi; t) = [A e^{j\zeta x} + B e^{-j\zeta x}] \cos q\phi J_q(\nu r) e^{j\omega t}. \quad (2.12)$$

With  $q$  constrained to be an integer.

The second and third are a result of the so called “no-penetration” boundary-condition of fluid-mechanics. It arises from the fact that the cavity wall is an impermeable boundary. This translates into the requirement that the normal velocity function should vanish ([28, p. 111]). The velocity function ( $\mathbf{v}$ ) is related to the pressure by,

$$-\rho \frac{\partial \mathbf{v}}{\partial t} = \nabla p \quad (2.13)$$

At the cylindrical cavity wall, the normal velocity is in the radial direction. Substituting the expression for pressure in (2.11) in the above equation leads to a Neumann boundary

condition for the pressure,

$$\begin{aligned} v_r &= -\frac{1}{j\rho\omega} \frac{\partial p(x, r, \phi; t)}{\partial r} \Big|_{r=a_{\text{cyl}}} = 0 \\ \Rightarrow \frac{\partial J_q(\nu r)}{\partial r} \Big|_{r=a_{\text{cyl}}} &= 0 \end{aligned} \quad (2.14)$$

This constrains  $\nu$  to a discrete set of values which correspond to the local minima and maxima of  $J_q$ . We can therefore index  $\nu$  by  $q$  and  $s = 0, 1, 2, 3, \dots$  with  $\nu_{qs} = z_{qs}/a_{\text{cyl}}$ :  $z_{qs}$  being the  $s^{\text{th}}$  extremum of the order- $q$  Bessel function of the first kind. This results in a discrete set of modes that satisfy (2.3) which are given by,

$$p_{qs}(x, r, \phi; t) = [A_{qs}e^{j\zeta_{qs}x} + B_{qs}e^{-j\zeta_{qs}x}] f_{qs}(r, \phi)e^{j\omega t} \quad (2.15)$$

where we have added the subscripts  $q$  and  $s$  to  $\zeta$  and denoted the  $(r, \phi)$  part of (2.12) by  $f_{qs}(r, \phi)$ . Effectively, the modes are 3D waves propagating with wave numbers  $\zeta_{qs}$  in the  $x$ -direction and  $\nu_{qs}$  in the radial direction. The first of these modes (corresponding to  $q = 0, s = 0$ ) is of particular importance. Since the first maximum of  $J_0$  occurs at  $r = 0$ , we have  $\nu_{00} = 0$ . This leads to the first mode being a plane-wave which is constant in  $r$  and  $\phi$  and only varies in  $x$ .

A very useful property of the above modes is their orthogonality, i.e.

$$\int_{\Omega} dV p_{q_1 s_1} p_{q_2 s_2} = 0, \text{ if } q_1 \neq q_2 \text{ or } s_1 \neq s_2 \quad (2.16)$$

the integral is over the volume of the cylinder. This is a consequence of the fact that for different  $q$ 's the cosine parts of the modes are orthogonal whereas for a given  $q$  the Bessel parts are orthogonal for different  $s$ 's or expressed as an equation,

$$\int dS f_{q_1 s_1} f_{q_2 s_2} = 0, \text{ if } q_1 \neq q_2 \text{ or } s_1 \neq s_2 \quad (2.17)$$

where  $dS = rdrd\phi$  and the integral being taken over the disk of radius  $a_{\text{cyl}}$ . We can therefore write the general solution to (2.3) as a linear combination of the orthogonal modes given in (2.15),

$$p(x, r, \phi; t) = \sum_{q=0}^{\infty} \sum_{s=0}^{\infty} (A_{qs}e^{j\zeta_{qs}x} + B_{qs}e^{-j\zeta_{qs}x}) f_{qs}(r, \phi)e^{j\omega t} \quad (2.18)$$

The remaining coefficients,  $A_{qs}$  and  $B_{qs}$ , will be determined by equating the velocity function to the membrane velocity at both ends of the cylinder. To do so, we will first need to find an expression for the membrane vibrations - as we will in the following section.

### 2.2.2 Vibration of the Membrane

As a preliminary exercise, we will first derive expressions for the free and force-driven vibrations of a circular membrane. We will then use our results to move on to the sectoral membrane which corresponds to the tympanum loaded by the extracolumella. This corresponds to the approximating the extracolumella to have infinite mass.

### Circular Membrane

The equation of motion for the vibration of a rigidly clamped circular membrane of radius  $a_M$  solves for the membrane displacement  $u$  at a point  $(r, \phi)$  with  $r < a$  and  $0 < \phi < 2\pi$ . It is given by,

$$\begin{aligned} -\frac{\partial^2 u(r, \phi; t)}{\partial t^2} - 2\alpha \frac{\partial u(r, \phi; t)}{\partial t} + c_M^2 \left[ \frac{1}{r} \frac{\partial}{\partial r} \left( r \frac{\partial u(r, \phi, t)}{\partial r} \right) + \frac{1}{r^2} \frac{\partial^2 u(r, \phi, t)}{\partial \phi^2} \right] \\ = \frac{1}{\rho_M d} \Psi(r, \phi; t) \end{aligned} \quad (2.19)$$

subject to the boundary condition  $u(r, \phi; t)|_{r=a_M} = 0$ . We've defined the following membrane material properties,

- $c_M$  - propagation speed of vibrations.
- $\alpha (> 0)$  - the damping coefficient.
- $\rho_M$  - density.
- $d$  - thickness.

$\Psi(r, \phi; t)$  is the pressure on the membrane surface at  $(r, \phi)$ . In our discussion we are only concerned with periodic and uniform pressure acting on the membrane surface. As we have already stated in Sec. 2.1.3, the small size of the membrane with respect to the sound wavelength, justifies the spatial uniformity of our input.

### Free Vibrations

**Undamped Membrane:** We first determine the eigenmodes of an undamped circular membrane by solving (2.19) for  $\alpha = 0$ ,  $\Psi = 0$  (the resultant equation is better known as the 2D Helmholtz equation, cf. [29, p. 187]). Just as we did in (2.4), we do this by making a separation ansatz ,

$$u(r, \phi; t) = f(r)g(\phi)h(t) \quad (2.20)$$

This gives us the following set of equations

$$\frac{\partial^2 f(r)}{\partial r^2} + \frac{1}{r} \frac{\partial f(r)}{\partial r} + \left[ \mu^2 - \frac{m^2}{r^2} \right] f(r) = 0 \quad (2.21)$$

$$\frac{d^2 g(\phi)}{d\phi^2} + m^2 g(\phi) = 0 \quad (2.22)$$

$$\frac{d^2 h(t)}{dt^2} + c_M^2 \mu^2 h(t) = 0 \quad (2.23)$$

with separation constants  $\mu$  and  $m$ . The solution of the first of these equations should already be familiar to us from the previous section -  $J_m(\mu r)$ , the order- $m$  Bessel function of the first kind. The boundary conditions in  $\phi$  direction remain the same resulting in,

$$u(r, \phi; t) = [(M^+ e^{jm\phi} + M^- e^{-jm\phi}) e^{jc_M \mu t} + (N^+ e^{jm\phi} + N^- e^{-jm\phi}) e^{-jc_M \mu t}] J_m(\mu r) \quad (2.24)$$

Unlike in the case of the internal cavity, we require  $u$  to vanish at the boundary so we have a Dirichlet boundary condition which effectively requires:  $J_m(\mu a_M) = 0$ . This constrains  $\mu$  to a discrete set of values which correspond to the zeros of  $J_m$ . The eigenmodes of a the circular membrane are therefore given by,

$$u_{mn}(r, \phi; t) = [(M_{mn}^+ e^{jm\phi} + M_{mn}^- e^{-jm\phi}) e^{j\omega_{mn}t} + (N_{mn}^+ e^{jm\phi} + N_{mn}^- e^{-jm\phi}) e^{-j\omega_{mn}t}] J_m(\mu_{mn} r) \quad (2.25)$$

where  $\mu_{mn} = z_{mn}/a_M$ ,  $z_{mn}$  being the  $n^{th}$  zero of  $J_m$  and,  $\omega_{mn} = c_M \mu_{mn}$  is the eigenfrequency of the  $(m, n)$  eigenmode. At this point  $m$  can take any positive real value – a fact that will help us solve the sectoral membrane problem. However, in the case of a full circular membrane – as in the case of the pressure inside a cylindrical cavity – requirements of continuity and smoothness in  $\phi$  reduce (2.25) to,

$$u_{mn}(r, \phi; t) = \cos m\phi J_m(\mu_{mn} r) [M_{mn} e^{j\omega_{mn}t} + N_{mn} e^{-j\omega_{mn}t}] \quad (2.26)$$

with  $m = 0, 1, 2, \dots$  with the  $(m, n)$  eigenmodes forming an orthogonal set. For later convenience we denote the spatial part of the above mode by  $u_{mn}(r, \phi)$ . The first few of these modes are plotted in 2.8.

We note that unlike in the case of the internal cavity, the free membrane has components that are both forward- and backward-moving in time. The presence of a driving force, however, will result in simpler expressions. This will be discussed in more detail in the next chapter where we compare our model with experimental data.

**Damped Membrane:** For a damped membrane, i.e.  $\alpha \neq 0$ , the spatial part of the above eigenmodes remains the same. The form of the time-dependent part is given by the solution of the equation,

$$\frac{d^2 h_{mn}(t)}{dt^2} + 2\alpha \frac{dh_{mn}(t)}{dt} + \omega_{mn}^2 h_{mn}(t) = 0. \quad (2.27)$$

Assuming  $h_{mn}$  takes the form  $e^{j\tilde{\omega}_{mn}}$  leads to a quadratic equation with solutions,

$$\tilde{\omega}_{mn} = j\alpha \pm \omega_{mn}^* \quad (2.28)$$

$$\omega_{mn}^* = \sqrt{\alpha^2 + \omega_{mn}^2} \quad (2.29)$$

We require the membrane displacement to remain finite as  $t \rightarrow \infty$ . We can therefore neglect the  $e^{-j\tilde{\omega}_{mn}}$  terms leading to,

$$\tilde{u}_{mn}(r, \phi; t) = \cos m\phi J_m(\mu_{mn} r) [M_{mn} e^{j\omega_{mn}^* t} + N_{mn} e^{-j\omega_{mn}^* t}] e^{-\alpha t} \quad (2.30)$$

The general solution is given by a linear combination of the above and the coefficients are determined by initial conditions – for example, membrane displacement and velocity at  $t = 0$ .

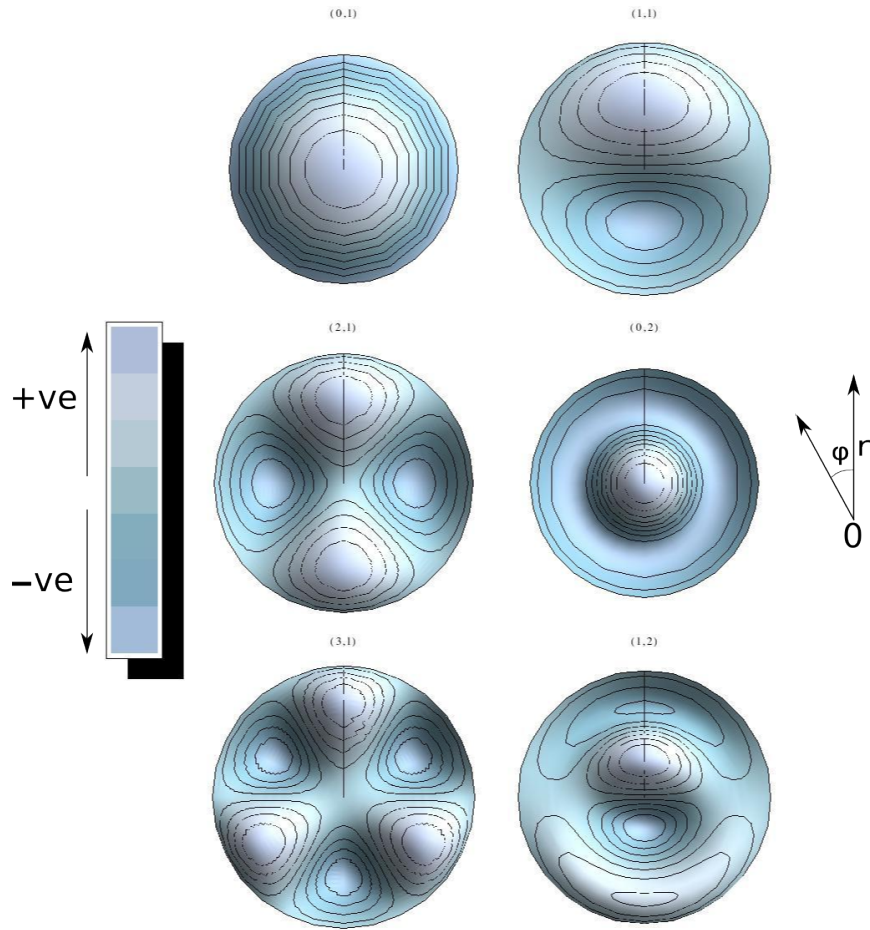


Figure 2.8: Eigenmodes of a full circular membrane with the eigennumbers of the modes shown above each figure. Displacements into the surface of the paper are darkly shaded while those out are lightly shaded (illustrated in the legend). The eigenfrequency increases from left to right.

### Forced Vibrations

For a periodically driven membrane, there are two components of the full solution for forced vibrations. The first of these is the steady state solution which oscillates with the same frequency as the input and does not depend on the initial conditions -  $u_{ss}$ . The second of these is the transient solution that depends on the initial conditions but not on the driving pressure -  $u_t$ .

**Steady State Solution:** The steady state solution is expressed as a linear combination of the spatial part of the above eigenmodes and is given by,

$$u_{ss}(r, \phi; t) = \sum_{m=0}^{\infty} \sum_{n=1}^{\infty} C_{mn} \cos m\phi J_m(\mu_{mn}r) e^{j\omega t}. \quad (2.31)$$

Substituting this expression in (2.19) with  $\Psi = pe^{j\omega t}$  gives,

$$\sum_{m=0}^{\infty} \sum_{n=1}^{\infty} \Omega_{mn} C_{mn} \cos m\phi J_m(\mu_{mn}r) e^{j\omega t} = pe^{j\omega t} \quad (2.32)$$

$$\text{where, } \Omega_{mn} = \rho_M d [(\omega^2 - \omega_{mn}^2) - 2j\alpha\omega]. \quad (2.33)$$

Using the orthogonality of the eigenmodes, the coefficients  $C_{mn}$  can be calculated,

$$C_{mn} = \frac{p \int dS u_{mn}}{\Omega_{mn} \int dS u_{mn}^2} \quad (2.34)$$

with the integral this time being taken over the circular disk of radius  $a_M$ .

**Transient Solution:** The transient solution is effectively a solution of the free damped membrane, i.e. a linear combination of the eigenmodes given in (2.30). Therefore,

$$u_t(r, \phi; t) = \sum_{m=0}^{\infty} \sum_{n=1}^{\infty} \cos m\phi J_m(\mu_{mn}r) [M_{mn} e^{j\omega_{mn}^* t} + N_{mn} e^{-j\omega_{mn}^* t}] e^{-\alpha t}. \quad (2.35)$$

The complete solution is given by  $u = u_t + u_{ss}$  and the coefficients  $M_{mn}$  and  $N_{mn}$  are determined by the initial conditions (at  $t = 0$ ).

**Steady State Approximation:** The damping coefficient  $\alpha$  is usually given in terms of the membrane fundamental frequency and a quality factor  $Q$  as  $\alpha = \omega_{01}/2Q$ . The tympani we will be concerned with are generally underdamped to critically damped i.e.  $Q \geq .5$  which results in damping coefficients that are around  $2400s^{-1}$  for the larger lizards and around  $7700s^{-1}$  for the smaller ones (the exact parameter values will be discussed in the next chapter). Due to this and the exponential decay of the transient vibration amplitude, we can safely assume that within a few time-periods the transient vibrations forced membrane will be negligible. For this reason, we will subsequently confine our discussion to only the steady state vibrations of the membrane.

### Sectoral Membrane

The eigenmodes of the sectoral membrane proceeds from (2.25) onwards. We now have a new set of boundary conditions in  $\phi$ . The extracolumella is modelled as a triangular plate of infinite mass which constrains the membrane displacement to go to zero at  $\phi = \beta$  and  $\phi = 2\pi - \beta$ . This results in the following set of eigenmodes,

$$u_{mn}(r, \phi; t) = \sin \kappa(\phi - \beta) J_\kappa(\mu_{mn}r) [M_{mn} e^{j\omega_{mn}t} + N_{mn} e^{-j\omega_{mn}t}] \quad (2.36)$$

where  $\kappa[m] = \frac{m\pi}{2(\pi - \beta)}$ ,  $m = 1, 2, 3, \dots$ . We see that the  $r$  part of the above mode is given by the order- $\kappa$  Bessel function of the first kind;  $\mu_{mn}$  being its  $n^{th}$  zero, as before. The solution for the damped membrane follows in an identical way. It is apparent from the

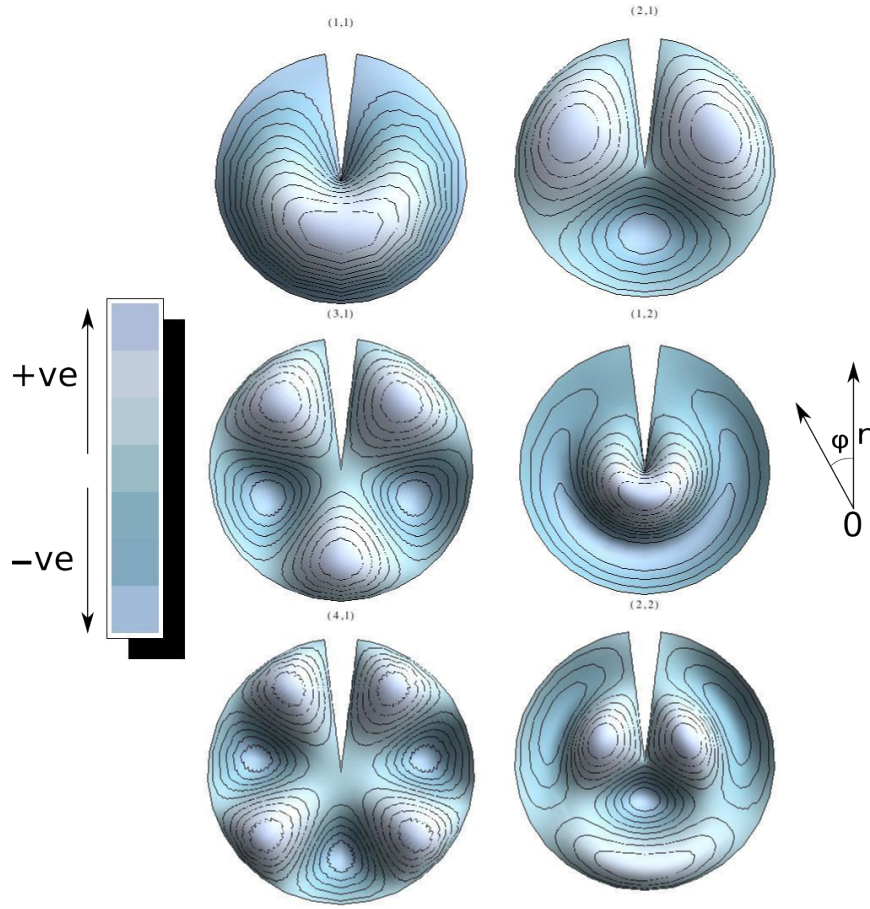


Figure 2.9: Eigenmodes of a sectoral membrane where the omitted region corresponds to the extracolumnella with  $\beta = \pi/25$ . The eigennumbers are shown above each figure. As in Fig. 2.8 displacements into the surface of the paper are darkly shaded while those out are lightly shaded. The eigenfrequency increases from left to right.

form of the above modes that, unlike in the case of the circular membrane eigenmodes, these modes are no longer circularly symmetric. We plot the first few of these modes in 2.9. The solution for forced membrane vibrations follows in the same way as in the circular membrane case. The vibrations of a sectoral membrane are discussed in more detail in [30, p. 87]. As discussed earlier, the sectoral shape of the membrane has important physical consequences and captures the complex vibration patterns of a realistic membrane. This will be discussed in the next chapter.

### 2.2.3 Vibration of Coupled Membranes

With our current knowledge, we can move on to the main part of the chapter - the vibration of coupled membranes. The derivation of the in this section is based on the treatment of the vibration of a circular membrane backed by a cylindrical air cavity closed at the opposite

end by Rajalingham *et al.*, [31]. The quantities of interest there were the eigenmodes of the circular membrane but in our analysis we are interested in the steady state vibration of the membranes. It is convenient to first write down the main equations of the system based on our previously derived expressions. The vibrations of the membranes is given by,

$$u_{0/L}(r, \phi; t) = \sum_{m=0}^{\infty} \sum_{n=1}^{\infty} \Omega_{mn} C_{mn}^{0/L} u_{mn}(r, \phi) e^{j\omega t} = p_{0/L} e^{j\omega t} - p(0/L, r, \phi; t) \quad (2.37)$$

where 0 and  $L$  denote the  $x = 0$  and  $x = L$  membranes respectively and the cavity pressure distribution,  $p(x, r, \phi; t)$ , is given by (2.18). The above equation is only valid on the membrane surface i.e., for  $r < a_{\text{typ}}$  and  $\beta < \phi < 2\pi - \beta$ .

As discussed in 2.2.1, the internal cavity pressure satisfies the no-penetration condition at solid boundaries. This means that at both ends of the cylinder, we equate the velocity profile of air to the velocity profile of the circular surface including the membrane. This is because the membrane diameter is smaller than the cylinder diameter. As a result, we will have to set the air-particle velocity to zero for  $r > a_{\text{typ}}$ . Since the membrane displacement is only in the  $x$ -direction, we only need to calculate the same component of the velocity. Using the relation (2.13) we get,

$$v_x(x, r, \phi; t) = -\frac{1}{\rho\omega} \sum_{q=0}^{\infty} \sum_{s=0}^{\infty} \zeta_{qs} (A_{qs} e^{j\zeta_{qs} x} - B_{qs} e^{-j\zeta_{qs} x}) f_{qs}(r, \phi) e^{j\omega t} \quad (2.38)$$

and the exact boundary conditions are given by,

$$j\omega U_0 = -v_x(0, r, \phi; t) \quad (2.39)$$

$$j\omega U_L = v_x(L, r, \phi; t) \quad (2.40)$$

where we've used the direction conventions described in 2.1 and made the following definition,

$$U_{0/L} = \begin{cases} u_{0/L}, & 0 < r < a_{\text{typ}} \text{ and } \beta < \phi < 2\pi - \beta \\ 0, & \text{otherwise} \end{cases} . \quad (2.41)$$

This in order to ensure that the boundary condition is satisfied over either end of the cylinder and not just over the membrane surface.

### Approximate Boundary Condition

As previously stated, the exact boundary condition would entail setting the velocity function to be exactly equal to the membrane displacement velocity. At this point, it is important to note that the internal cavity eigenmodes are **not** orthogonal to the membrane eigenmodes in general<sup>2</sup>. This means that every membrane eigenmode couples with every

---

<sup>2</sup>This would also be true if we had full circular membranes on either end of the cylinder. In this case we would have the added simplification that only the circularly symmetric cavity eigenmodes will be activated.

cavity eigenmode and that each of the coefficients  $A_{qs}$  and  $B_{qs}$  will be given by an infinite linear combination of the coefficients  $C_{mn}^{0/L}$ .

The first step in overcoming this problem is to rewrite the left-hand sides of the boundary conditions given in (2.39) and (2.40). We first expand  $U_0$  and  $U_L$  in the orthogonal basis of the functions  $f_{qs}$ ,

$$U_{0/L}(r, \phi; t) = \sum_{q=0}^{\infty} \sum_{s=0}^{\infty} S_{qs}^{0/L} f_{qs}(r, \phi) e^{j\omega t} \quad (2.42)$$

$$\text{where, } S_{qs}^{0/L} = \frac{\int dS U^{0/L} f_{qs}(r, \phi)}{\int dS f_{qs}^2(r, \phi)} \quad (2.43)$$

We now have an expansion that approximates the boundary condition with increasing accuracy. After choosing an appropriate cutoff for the expansion we can substitute this expression in place of  $U_{0/L}$  in (2.39) and (2.40). In fact, this cutoff in the boundary condition expansion results in an identical cutoff in the pressure expansion - a direct result of the orthogonality of the pressure modes.

We will now illustrate a solution to the problem by solving the problem with the zeroeth order boundary conditions. In the end, it will turn out that for our purposes the zeroeth order, i.e. the  $(0, 0)$  mode is sufficient as higher modes only have a significant contribution at frequencies well above the hearing range of geckos. For example, the wavenumber of the  $(1, 1)$  mode is above 33kHz for the cylindrical cavity corresponding to the house gecko and above 15kHz for the one corresponding to the Tokay gecko. The parameters used to derive these quantities will be discussed in the next chapter. We can therefore write the approximate boundary conditions to zeroeth order as,

$$\rho\omega^2 S^0 = - \sum_{q=0}^{\infty} \sum_{s=0}^{\infty} j\zeta_{qs} (A_{qs} - B_{qs}) f_{qs}(r, \phi) \quad (2.44)$$

$$\rho\omega^2 S^L = \sum_{q=0}^{\infty} \sum_{s=0}^{\infty} j\zeta_{qs} (A_{qs} e^{j\zeta_{qs} L} - B_{qs} e^{-j\zeta_{qs} L}) f_{qs}(r, \phi) \quad (2.45)$$

As shown in Sec. 2.2.1, the  $(0, 0)$  mode only varies in the  $x$ -direction. As a result, the left-hand sides of the above equation are nothing but the average displacement of the membrane surface given by,

$$S^{0/L} = \frac{\int dS U^{0/L}(r, \phi)}{\pi a_{cyl}^2}. \quad (2.46)$$

We have also omitted the “ $qs$ ” subscript from  $S^{0/L}$ . Given the external parameters and boundary conditions, it only depends on time. We have effectively approximated the surfaces at 0 and  $L$  (including the membranes) by pistons moving with the average velocity of the total surface.

Given these boundary conditions, it is straightforward to calculate the coefficients  $A_{qs}$  and  $B_{qs}$  in terms of  $S_{0/L}$ . To do this we need to make use of the orthogonality relation

given in (2.17). We do this by multiplying both sides of (2.44) and (2.45) by  $f_{qs}(r, \phi)$  and integrate over the circular surfaces at either end of the cylinder. This results in a system of two linear equations for each pair of  $A_{qs}$  and  $B_{qs}$ ,

$$A_{qs} - B_{qs} = -L_{qs}\rho\omega^2 S^0 \quad (2.47)$$

$$A_{qs}e^{j\zeta_{qs}L} - B_{qs}e^{-j\zeta_{qs}L} = L_{qs}\rho\omega^2 S^L \quad (2.48)$$

$$\text{where, } L_{qs} = \frac{\int dS f_{qs}(r, \phi)}{j\zeta_{qs} \int dS f_{qs}^2(r, \phi)}$$

We now make use of the property of the pressure modes that  $f_{qs}(r, \phi)$  integrates to 0 unless  $q = 0$  and  $s = 0$ . For  $q = 0$  this is a consequence of the Bessel functions integrating to zero while for  $q \geq 1$  this is due to the more obvious fact that the integral of the cosine function from 0 to  $2\pi$  is zero. As a result we have  $A_{qs} = B_{qs} = 0$  for all modes except the  $(0,0)$  mode. In other words, the zeroeth-order boundary condition only supports plane wave modes inside the cavity. We will subsequently omit the subscripts “00” for these coefficients. From the above linear equations, they are given in terms of the total membrane displacement as,

$$A = -\frac{\rho\omega^2}{2k \sin kL} (S^0 e^{-jkL} + S^L), \quad B = -\frac{\rho\omega^2}{2k \sin kL} (S^0 e^{jkL} + S^L) \quad (2.49)$$

we have also directly substituted  $\zeta_{00} = k$  and simplified the expression for  $K_{00}$  in the above expressions. These coefficients can now be substituted in place of the pressure in the right-hand side of the equation (2.37) giving us,

$$\sum_{m=0}^{\infty} \sum_{n=1}^{\infty} \Omega_{mn} C_{mn}^0 u_{mn}(r, \phi) = p_0 + \frac{\rho\omega^2}{k} (S^0 \cot kL + S^L \csc kL) \quad (2.50)$$

$$\sum_{m=0}^{\infty} \sum_{n=1}^{\infty} \Omega_{mn} C_{mn}^L u_{mn}(r, \phi) = p_L + \frac{\rho\omega^2}{k} (S^0 \csc kL + S^L \cot kL) \quad (2.51)$$

where we have cancelled out the time component on both sides of the equations. Note that the right-hand sides of the above two equations are independent of the spatial  $(r, \phi)$  coordinates.

In order to simplify the above coupled system of equations, the next step will be to take their sum and difference to obtain a new set of variables that are solutions of a pair of decoupled equations. After some algebraic manipulation, we therefore have

$$\sum_{m=0}^{\infty} \sum_{n=1}^{\infty} \Omega_{mn} C_{mn}^+ u_{mn}(r, \phi) = p_+ + \frac{\rho\omega^2}{k} S^+ \cot \frac{kL}{2} \quad (2.52)$$

$$\sum_{m=0}^{\infty} \sum_{n=1}^{\infty} \Omega_{mn} C_{mn}^- u_{mn}(r, \phi) = p_- - \frac{\rho\omega^2}{k} S^- \tan \frac{kL}{2} \quad (2.53)$$

where,  $C_{mn}^+ = C_{mn}^L + C_{mn}^0$  and  $C_{mn}^- = C_{mn}^L - C_{mn}^0$ . The  $S^{+/-}$  and  $p_{+/-}$  terms are defined similarly. Now, analogous to the calculation of the coefficients for the steady state vibration in (2.32) and (2.34), we can determine the coefficients of the sum and difference vibrations in terms of the pressure and total membrane displacements. This gives us,

$$C_{mn}^+ = \left[ p_+ + \frac{\rho\omega^2}{k} S^+ \cot \frac{kL}{2} \right] \frac{K_{mn}}{\Omega_{mn}} \quad (2.54)$$

$$C_{mn}^- = \left[ p_- - \frac{\rho\omega^2}{k} S^- \tan \frac{kL}{2} \right] \frac{K_{mn}}{\Omega_{mn}} \quad (2.55)$$

$$\text{where, } K_{mn} = \frac{\int dS u_{mn}}{\int dS u_{mn}^2} \quad (2.56)$$

The next step will be to multiply both sides of (2.54) and (2.55) with the integral  $\int dS u_{mn}$ , divide by  $\pi a_{cyl}^2$  (the integral of  $f_{00}^2$  as it appears in the denominator in (2.43)) and sum over  $m$  and  $n$ . It is clear that the left hand sides become equal to  $S^{+/-}$ ; this allows us to give exact expressions for the total membrane displacements.

$$S^+ = \frac{p_L + p_0}{\Lambda + \Gamma_+} \quad S^- = \frac{p_L - p_0}{\Lambda + \Gamma_-} \quad (2.57)$$

where we've defined the following quantities,

$$\Gamma_+ = -\frac{\rho\omega^2}{k} \cot \frac{kL}{2}, \quad \Gamma_- = \frac{\rho\omega^2}{k} \tan \frac{kL}{2} \quad (2.58)$$

$$\frac{1}{\Lambda} = \sum_{m=0}^{\infty} \sum_{n=1}^{\infty} \frac{K_{mn}}{\pi a_{cyl}^2 \Omega_{mn}} \quad (2.59)$$

The  $\Gamma_{\pm}$  terms contain the effect of the coupling through the air cavity and  $1/\Lambda$  is the response of the membrane to a unit pressure of angular frequency  $\omega$ . We can finally write the membrane displacement as a function of the pressure inputs in the form

$$u_0(r, \phi; t) = G_{ipsi}(r, \phi)p_0 + G_{contra}(r, \phi)p_L \quad (2.60)$$

$$u_L(r, \phi; t) = G_{contra}(r, \phi)p_0 + G_{ipsi}(r, \phi)p_L \quad (2.61)$$

with the ipsilateral filter,

$$G_{ipsi} = \left( \frac{1}{\Lambda + \Gamma_+} + \frac{1}{\Lambda + \Gamma_-} \right) \sum_{n=1}^{\infty} \frac{\Lambda K_{mn}}{2} u_{mn}(r, \phi; t) \quad (2.62)$$

and the contralateral filter,

$$G_{contra} = \left( \frac{1}{\Lambda + \Gamma_+} - \frac{1}{\Lambda + \Gamma_-} \right) \sum_{n=1}^{\infty} \frac{\Lambda K_{mn}}{2} u_{mn}(r, \phi; t) \quad (2.63)$$

The total membrane displacement can also be expressed as a function of  $p_0$  and  $p_L$  simply by integrating both sides of (2.60) and (2.61) giving us a new set of ipsi- and contralateral filters

$$G_{ipsi}^s = \left( \frac{1}{\Lambda + \Gamma_+} + \frac{1}{\Lambda + \Gamma_-} \right) / 2 \quad (2.64)$$

$$G_{contra}^s = \left( \frac{1}{\Lambda + \Gamma_+} - \frac{1}{\Lambda + \Gamma_-} \right) / 2 \quad (2.65)$$

The ipsilateral filter effectively gives us the response of the membrane to a purely ipsilateral stimulus or equivalently when the contralateral membrane is blocked. Similarly, the contralateral filter gives us its response when the ipsilateral membrane is blocked. These filters will play an important role in the evaluation of the model in the next chapter. Before we move on it is important to note that since  $\Lambda$  is an infinite series, in numerical analyzes it has to be approximated by choosing an appropriate membrane mode cutoff. The choice of this cutoff depends on parameters specific to the animal; cf. Sec. 3.1.3. The basic method involves arranging the modes in increasing order of eigenfrequency (or equivalently  $\mu_{mn}$ ). As a result, we can express the summation over a single index. In general, for the frequency ranges of the animals we are concerned with, we will not need to calculate the summation beyond the the first 30 eigenmodes.

### 2.2.4 Circuit Model

Before we conclude this chapter, we will discuss the previous methods used to model ears coupled through an air cavity. This method was used by Christensen-Dalsgaard and Manley in [4] and [21] and Zhang *et al* in [32]. It was based on methods presented in [30]. The method treats the problem through the analogy of electrical circuits and deals with low-frequency and high-frequency regimes separately.

In these models, the sound inputs are treated as voltage sources and the system is broken down into components, e.g. membranes, cavities, apertures which are modelled as lumped elements. Their impedance values depend on the geometry and material properties and in general can be resistive and reactive. The “current” is given by something called the “acoustic flow” which has the dimensions of volume per unit time. In the previous analysis, this is given by  $j\omega\pi a_{cyl}^2 S^{0/L}$ .

The low frequency circuit analog for the ICE model is illustrated in Fig. 2.10. The impedances are calculated using the following formulae,

$$R_T = \frac{\omega_T L_T}{Q}, \quad L_T = \frac{\rho_M d}{\pi a_{tym}^2}, \quad C_T = \frac{1}{\omega_T^2 L_T} \quad (2.66)$$

$$R_V = 0, \quad L_V = 0, \quad C_V = \frac{V_{cav}}{\rho c^2} \quad (2.67)$$

where  $R$ ,  $L$  and  $C$  are the resistance, impedance and capacitance of the quantities respectively with the total impedance given by  $Z = R + j\omega L + 1/j\omega C$ .  $\omega_T$  is the first eigenfrequency of the membrane. It should immediately be apparent that the cavity impedance

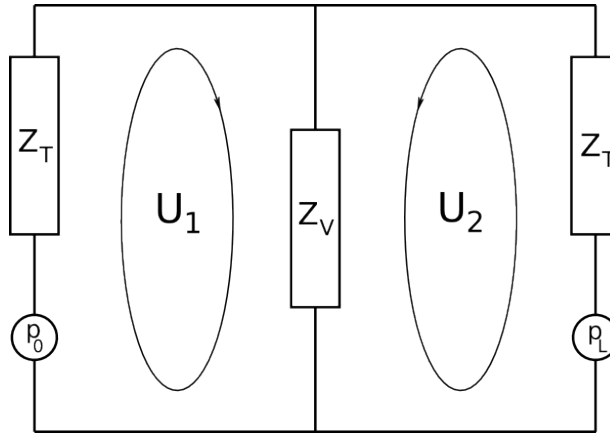


Figure 2.10: Low frequency circuit analog for the ICE Model. The membrane impedances are denoted by  $Z_T$  and the impedance of the internal cavity is denoted by  $Z_V$ . The acoustic flows are given by  $U_1$  and  $U_2$ .

only depends on its volume. This is a result of the assumption that the air inside the cavity behaves like an adiabatic gas. The adiabatic equation of state can then be used to determine the instantaneous pressure from the instantaneous volume change due to the membrane motion which, after linearization, results in a uniform pressure inside the cavity. In addition, the membrane impedance  $Z_T$  only includes the effect of the first eigenmode. Also,  $Z_T$  includes the effect of the transducer which, in our case, is the extracolumella. Upon solving the circuit equations, the acoustic flows are calculated to be,

$$U_1 = \frac{p_0(Z_T + Z_V) - p_L Z_V}{Z_T(Z_T + 2Z_V)}, \quad U_2 = \frac{p_L(Z_T + Z_V) - p_0 Z_V}{Z_T(Z_T + 2Z_V)}. \quad (2.68)$$

At first glance the above results look very similar to total membrane displacements shown in (2.60) and (2.61). In fact, we can find the equivalent impedances from our analysis by comparing  $U_0$  and  $U_L$  with the above results,

$$Z_T^{eq} = \frac{1}{j\omega\pi a_{cyl}^2}(\Lambda + \Gamma_-), \quad Z_V^{eq} = \frac{1}{2j\omega\pi a_{cyl}^2}(\Gamma_+ - \Gamma_-) \quad (2.69)$$

We immediately see that in the equivalent membrane impedance there is a correction term,  $\Gamma_-$ , which is a result of the contribution of the cavity whereas in the circuit model, the membrane impedance is determined independent of the cavity. Moreover, the equivalent standalone membrane impedance,  $\Lambda$ , includes the influence of the higher modes. The equivalent cavity impedance becomes equal to  $Z_V$  at zero frequency and goes to infinity at the resonance frequencies of the cylinder, i.e at  $\omega = n\pi c/L$ ,  $n = 1, 2, \dots$

We conclude this chapter by briefly stating the advantages of our method in comparison to the lumped element method -

- In terms of the membrane motion - we are able to account for the effect of asymmetrically loaded extracolumella rendering it possible to describe the membrane motion in spatial detail.

- At low frequencies our model is consistent with the uniform pressure assumption but the non-uniformity steadily increases with frequency. We therefore have a single model that can describe both high- and low-frequency behaviour instead of treating the two regimes separately.

# Chapter 3

## Evaluation of the Model

We now have a complete geometrical representation of the ICE model as well as the analytical expressions  $u_0$  and  $u_L$  that describe the membrane displacements in spatial detail as a function of direction and frequency. In this chapter we will use these variables to further study the features and predictions of our model and compare them with experimental results. In order to completely explain the observations, we will also need to estimate certain physical parameters like membrane eigenfrequency and quality factor that are important to our analysis but haven't yet been experimentally measured.

The main body of this chapter proceeds in Sec. 3.1 directly from the definitions given in (2.60) and (2.61). We will begin by assigning numerical values to the model parameters that have been defined in the previous chapter and comparing the membrane velocities of our model with experimentally determined values. We will then go on to define and study the two main quantities that serve as important localization cues - the Internal Time Differences (iTDS) and the Internal Level Differences (iLDs). These values model the possible neural subtractions that take place in the animal's brain in order to enhance directional sensitivity. Upon obtaining the spectral behaviour of these quantities, we will also be able to make an educated guess about the respective frequency ranges in which these cues are dominant and the possible range in which they could simultaneously be used. We will end this section by discussing possible methods to estimate parameter values that are difficult to measure. Finally, in Sec 3.2 we will compare the experimentally determined vibration pattern of the Tokay gecko's eardrum with that of our model's eardrum - the aim being to justify our choice for the geometry of the membrane.

In order to underline the fact that our model is universal model for internally coupled ears and not specialized to single species, we will compare our results for two gecko species - *Hemidactylus frenatus* or the common house gecko and the Tokay gecko. At the end of the chapter we will have an understanding of the advantages of a coupled system of ears as opposed to a pair of independent ears. We will also have an idea about the frequency regimes that correspond to the use of iTDs and iLDs in localization.

### 3.1 Sound Localization Using the ICE -Model

In our study we are primarily concerned with hearing in geckos. We will be using parameters (interaural separation, tympanum area etc.) from *Hemidactylus frenatus*, the common house gecko [21] and the Tokay gecko [4], [15]. In order to proceed with our evaluation of our model, we will need to assign appropriate numerical values to the parameters we have defined in 2.1. For now we will simply list the values and leave the discussion to a later point.

*Table 3.1: ICE Model geometry Parameters for the common house gecko (*Hemidactylus frenatus*) and the Tokay gecko.*

Parameter name	Hemidactylus	Tokay gecko
Length of the cylinder or interaural distance, $L$	10 mm	22 mm
Radius of the tympanic membrane, $a_{\text{tym}}^{\text{p}}$	1.6 mm	2.6 mm
Fundamental frequency (first eigenfrequency) of the tympanic membrane, $f_0 = \omega_{01}/2\pi$	2.8 kHz	1.05 kHz
Quality factor of the tympanum, $Q$	1.54	1.33
Density of the membrane material, $\rho_m$	1 mg/mm <sup>3</sup>	1 mg/mm <sup>3</sup>
Thickness of the membrane, $d$	8 $\mu\text{m}$	10 $\mu\text{m}$
Volume of the cavity, $V_{\text{cav}}$	.32 ml	3.5 ml
Extracolumella angle, $\beta$	$\pi/25$	$\pi/25$
Cylinder radius calculated from $V_{\text{cav}}$ and $L$ using the formula given in (2.1), $a_{\text{cyl}}$	$\sim 3.2$ mm	$\sim 6.6$ mm

From these quantities it should be apparent that the house gecko, with an interaural separation of 10 mm and mouth cavity volume of .32 ml is a rather small lizard. The Tokay gecko is the second largest gecko species (interaural separation of 22 mm and mouth cavity volume 3.5 ml, [21]). Thus we will demonstrate the scalability of our model with regards to hearing in animals with widely varying head widths and mouth cavities. As we will subsequently see, the geometric parameters, especially the head width and the membrane eigenfrequencies, put important limits on the “hearing range” of our model.

Before we begin our comparison of the data, we should first acquaint ourselves with some experimental details. As already mentioned in Sec. 2.1.3, the geckos were placed in an anechoic room. They were subject to 175 ms frequency sweeps (200-7500 Hz) at levels of 80-90 dB with the speakers placed at a 1 m distance. The eardrum vibrations were then measured using laser-Doppler vibrometry with the point of measurement at the tip of the extracolumella. The measured values correspond to the displacement velocity of the membrane at this point. In our analysis, the point corresponding to the tip of the extracolumella is stationary and cannot be used to compare the vibrations of the membranes. Instead, we use the total membrane displacements defined in the previous

chapter which are given by,

$$S^0 = G_{ipsi}^s p_0 + G_{contra}^s p_L \quad (3.1)$$

$$S^L = G_{ipsi}^s p_L + G_{contra}^s p_0 \quad (3.2)$$

$$\dot{S}^{0/L} = j\omega S^{0/L} \quad (3.3)$$

using the ipsi- and contralateral filters for the total displacement defined in (2.64) and (2.65). The definition of the total membrane velocity given in the second line follows directly from the definition of the membrane displacements. Following Sec. 2.1.3 and (2.2), the sound pressure inputs have the form

$$p_0 = pe^{j\omega t} e^{j\Delta_{new}/2}, \quad p_L = pe^{j\omega t} e^{-j\Delta_{new}/2}, \quad \Delta_{new} = 1.5kL \sin \theta. \quad (3.4)$$

The rest of this section follows from the above definitions. In Sec. 3.1.1 we study the dependence of the membrane vibration velocity on the frequency and direction of the sound source. Using the membrane vibration velocity we will define the main directional hearing cues - the Internal Time and Level Differences - in Sec. 3.1.2. As mentioned earlier, we will conclude by justifying our selection of parameters. In Sec. 3.1.3 we will analyze the dependence of the expressions defined in previous sections on the system parameters and in this way also provide estimates for realistic material parameters. The code used for all the subsequent simulations is given in A

### 3.1.1 Membrane Vibration Velocity

We will first evaluate the variation of the membrane displacements with respect to external sound stimuli. Before we begin, we should note that although the quantities  $\dot{S}^{0/L}$  will not quantitatively reproduce the experimentally measured membrane vibrations, their behaviour with respect to frequency and direction is consistent. They also have the added advantage that they only depend on direction and frequency. In Fig. 3.1, we compare the normalized velocity of the tympanic membrane ( $\dot{S}^{0/L}/(\pi a_{cyl}^2)$ ) with the membrane velocity measured using laser vibrometry in [4] and [21]. The plot shows the vibration amplitude as a function of frequency ( $y$ -axis) and direction ( $x$ -axis). The amplitudes are given in units of dB re 1 mm/(s Pa). This means that we have plotted the ratio vibration amplitude with reference to a vibration velocity of 1 mm/s with an input pressure of 1 Pa. In other words we have set  $p = 1$  Pa in (3.4).

As we can see, the total membrane velocities reproduce the frequency and direction dependence of the system fairly well. The directional behaviour is consistent with regard to the requirement that the membrane have a higher vibration amplitude when it is on the same side as the object. The reason for the deviation from experimental behaviour at higher frequencies isn't currently known. The mechanics of the extracolumella including its flexion and the influence of the realistic shape of the mouth cavity could offer possible explanations. Although the room was tested to be anechoic to below 200 Hz some reflections, especially from the laser setup are unavoidable. This is the cause of the spectral ripple in

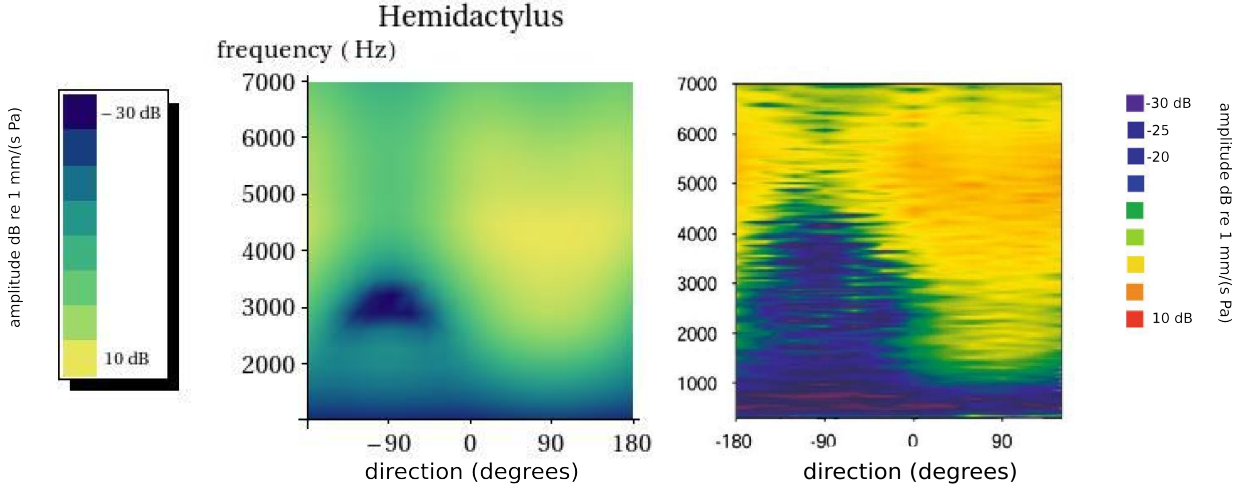


*Figure 3.1:* Calculated (left) and experimental (right) amplitude of tympanic membrane vibrations for *Hemidactylus frenatus* in dB re 1 mm/(s Pa), i.e. the ratio of the vibration amplitude with reference to a vibration velocity of 1 mm/s with an input pressure of 1 Pa. On the x-axis we have the direction of the sound source in degrees varying from  $-180^\circ$  to  $180^\circ$  with positive angles corresponding to ipsilateral stimuli. The legends on the left and right denote the amplitude in decibels. The calculated values are from the ICE model and the experimental values are taken from Christensen-Dalsgaard [21].

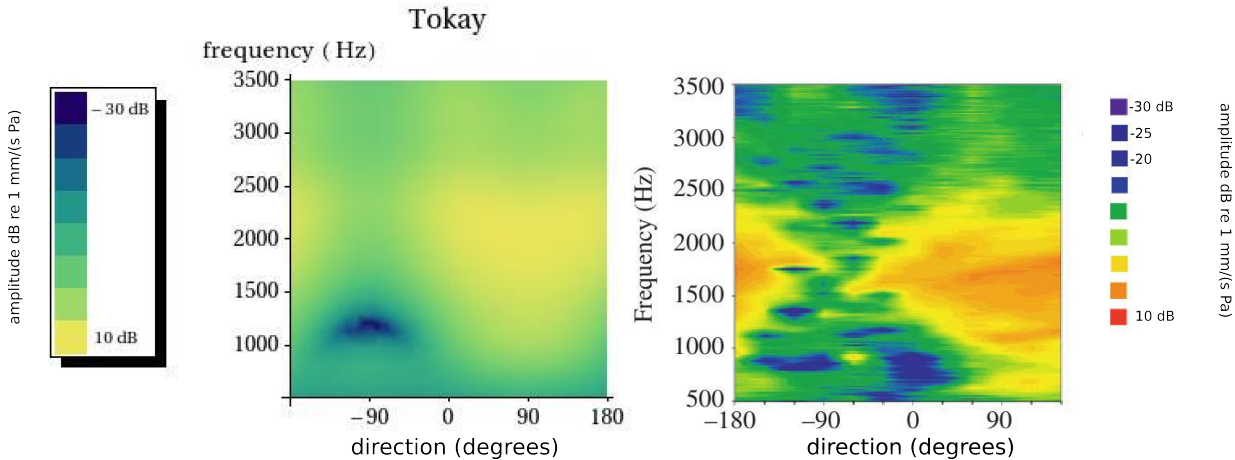


*Figure 3.2:* Calculated (left) and experimental (right) amplitude of tympanic membrane vibrations for the Tokay gecko in dB re 1 mm/(s Pa). The axis and legend values are the same as the ones in Fig. 3.1. The experimental values are taken from Christensen-Dalsgaard [4].

the experimental measurements. The same comparison is illustrated for the Tokay gecko in Fig. 3.2 (data from [4]).

In order to get a better understanding of the directionality of the model, it is also important to look at the dependence of the vibration amplitudes on direction and frequency independently. In Fig. 3.3 (house gecko) and Fig. 3.4 (Tokay gecko) we have plotted the

membrane vibration velocity for a pure ipsilateral stimulus ( $90^\circ$ ) and pure contralateral stimulus ( $-90^\circ$ ) as a function of frequency. As we can see the ipsilateral response is generally

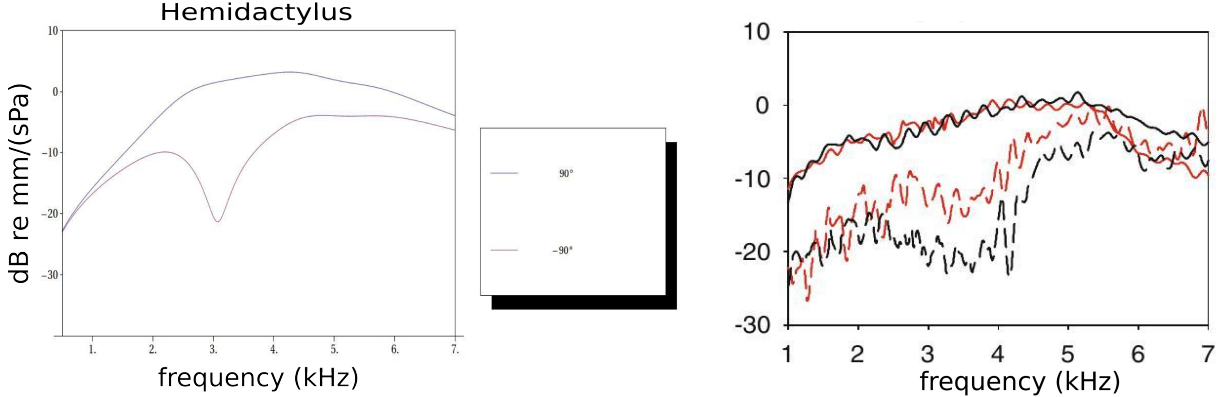


Figure 3.3: Calculated (left) and experimental (right) vibration velocity spectra for the common house gecko. The two plots on the left correspond to the response of the tympanic membrane to a purely ipsilateral ( $90^\circ$ ) and purely contralateral ( $-90^\circ$ ) stimulus. The two colours on the right correspond to different individuals of the house gecko species. Experimental values taken from Christensen-Dalsgaard [21].

higher than the contralateral response and the difference peaks at a certain frequency i.e., it has a bandpass characteristic which is consistent with observations. These amplitude differences can be used to localize the sound source; see Sec. 3.1.2. At very low and very high frequencies the both the vibration amplitudes converge. In Fig. 3.5 we have also plotted the response of the ear to ipsi- and contralateral stimuli with varying directions. ( $90^\circ, 60^\circ, 0^\circ, -60^\circ, -90^\circ$ ) and thereby shown that the vibration amplitude is higher when the sound source is nearer to the ear (i.e.  $\theta$  is closer to  $90^\circ$ ).

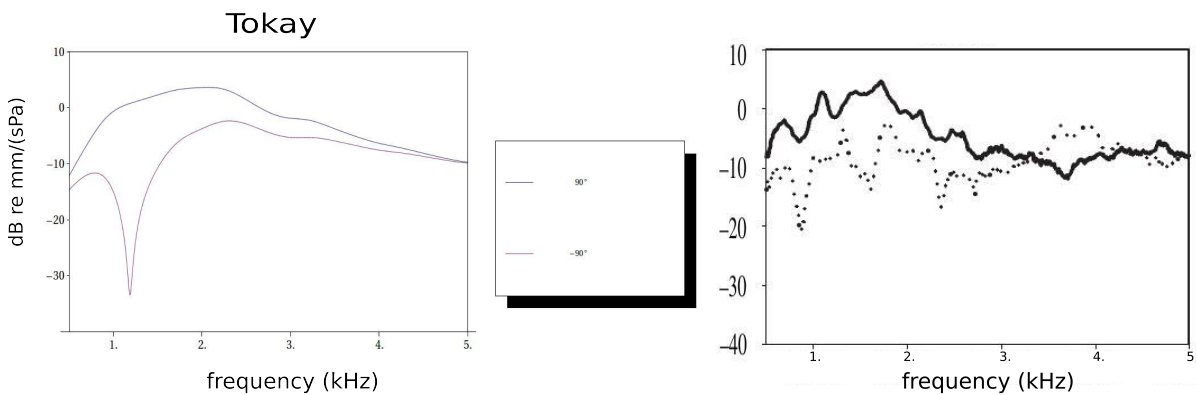
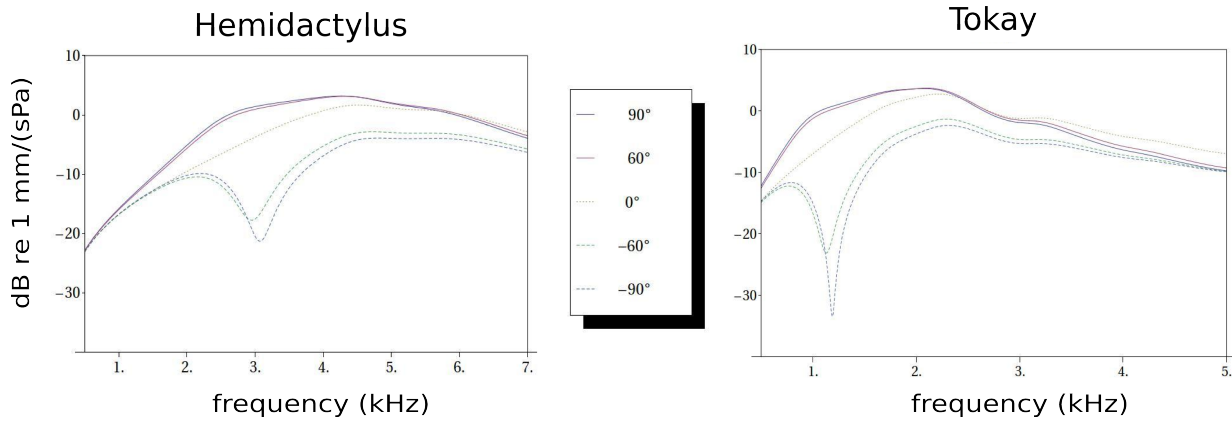


Figure 3.4: Calculated (left) and experimental (right) vibration velocity spectra for the Tokay gecko. In the plot on the right hand side, the thick line corresponds to an ipsilateral stimulus and the dotted line to a contralateral stimulus. Data from [4].



*Figure 3.5: Frequency dependence of membrane vibration amplitudes for different directions - common house gecko (left), Tokay gecko (right). The amplitude response to ipsilateral stimuli is generally higher and is at a maximum when the object is nearest to the ear i.e.  $\theta = 90^\circ$ . The dotted line denotes a sound source directly in front of or behind the animal and the dashed lines denote contralateral stimuli.*

We conclude this section by looking at the directional dependence of the vibration for a given set of frequencies. In Fig. 3.6, we show the variation of the vibration amplitude of the membrane as the sound source moves around the animal i.e. as  $\theta$  varies from  $-180^\circ$  to  $180^\circ$ . Here we can more clearly see that the amplitudes due to ipsilateral stimuli are higher than those due to contralateral stimuli. The marked asymmetry and the steepness across the midline (i.e. at  $0^\circ$ ) is also consistent with observations ([4], [21]). The choice of our frequencies has to do with the typical hearing ranges of the geckos. The smaller house gecko is most sensitive at higher frequencies ( 3 kHz) and the larger Tokay gecko at lower frequencies ( 1 kHz).

### 3.1.2 Directional Hearing Cues

The significance of our results up to this point should already be apparent. Due to the relatively small head sizes of the geckos, the sound arriving at the two ears differ very slightly in phase and not at all in amplitude. On the other hand these animals overcome the problem and create strongly directional membrane vibration amplitudes through the use of coupled ears. From form of the direction dependence of the membrane vibration amplitudes we see that individual amplitudes don't necessarily vary much with direction. In other words, although there is a clear difference between the ipsilateral and contralateral response, the difference between a given pair of ipsi- or contralateral directions (eg. between  $90^\circ$  and  $75^\circ$  or between  $-90^\circ$  and  $-70^\circ$ ) isn't very significant. Moreover, for some frequencies it seems that the vibration amplitude is lower at  $\theta = 90^\circ$  than at  $\theta \sim 60^\circ$ . As a result of this, the vibration amplitudes of the ears cannot be independently used to localize the objects. In order to do so by using the tympanic membrane vibration amplitudes, we need to compare the variation of their differences with respect to direction. We therefore need functions that accurately quantify the directional dependence of the system at a given frequency.

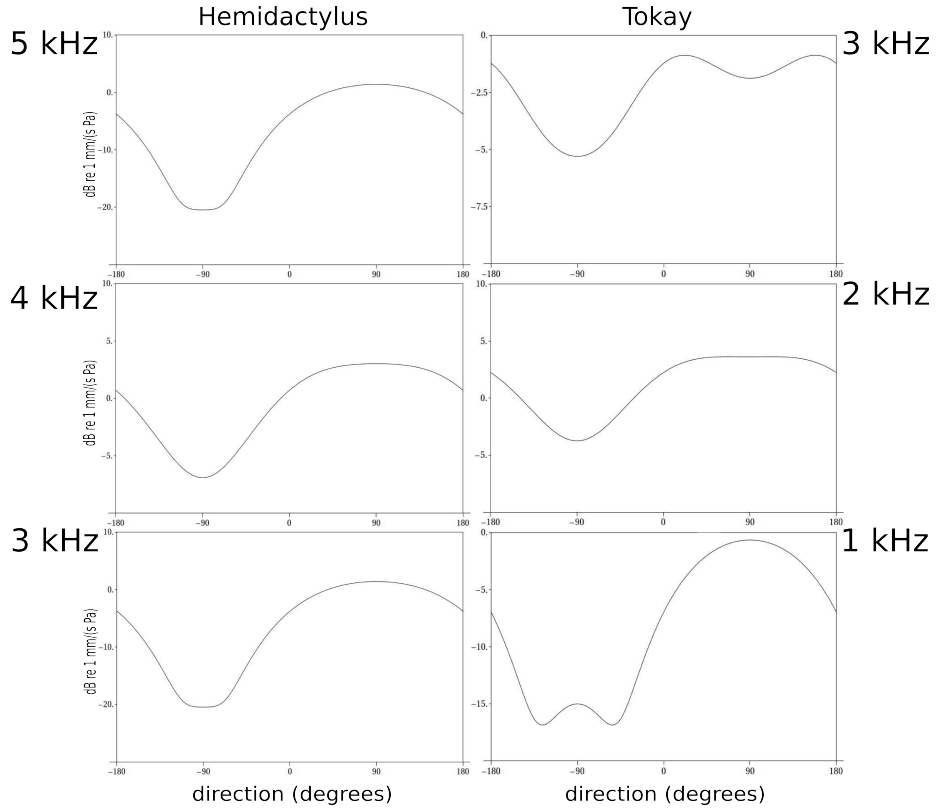


*Figure 3.6: Direction dependence of membrane vibration amplitudes (dB re 1 mm/(s Pa)) in the ICE Model for different frequencies - common house gecko (left, at 3kHz, 4kHz and 5kHz), Tokay gecko (right, at 1 kHz, 2 kHz and 3 kHz). The variation of the amplitude as the sound source completes a full circle around the animal is illustrated. The amplitudes for ipsilateral stimuli are shown to be higher than those for contralateral stimuli.*

As a first step we define the two quantities that are the main focus of this chapter - the internal level difference (iLD) and internal time difference (iTID) in terms of the total membrane velocities.

$$\text{iLD} := 20 \log_{10} \left( \left| \frac{\dot{S}^0}{\dot{S}^L} \right| \right) \quad (3.5)$$

$$\text{iTD} := \text{Arg} \left( \frac{\dot{S}^0}{\dot{S}^L} \right) / \omega. \quad (3.6)$$

Due to the steady state approximation we have the added advantage that the ratio of the displacement amplitudes is equal to that of the velocity amplitudes; see (2.31). The main advantage of the velocity amplitudes is their relative ease of measurement in experiments. The iLD measures the ratio between the amplitudes of the eardrums and is the same as the IVAD function defined by Jørgensen *et al.* [33] and is measured in dB. The iLD is positive for ipsilateral directions and negative for contralateral. This agrees with observed behaviour and means that the response of the system is directional. The iTD corresponds

to the time difference (or equivalently phase difference) between the membrane vibrations. The ipsilateral ear is always ahead in phase with respect to the contralateral ear. This means that it is negative for ipsilateral directions and positive for contralateral.

The iTD and iLD can be seen as the output of the ICE system with  $p_0$  and  $p_L$  as inputs. In contrast, the Interaural Time and Level Differences (ITD and ILD) are entirely determined by the inputs to the two ears. The ITD is defined as the time difference between the vibrations between the vibrations of the eardrums in the absence of coupling. It is calculated from the phase difference between the inputs at both ears; see (2.2)

$$\text{ITD} = \frac{\text{Arg}(pL/p0)}{\omega} = 1.5 \frac{L}{c} \quad (3.7)$$

Due to the input pressures having the same amplitude and due to the linearity of the system (w.r.t sound input), in the absence of coupling the membranes of the ICE model cannot have any a priori Interaural Level Difference. In larger animals like humans the difference between the input amplitudes increases with frequency due to diffraction effects (shadowing) which aids in localization; cf. [30, p. 154]. In addition, the gain in ITD due to their increased head size also provides sufficient information for localization at lower frequencies.

In order to effectively function as cues for localization the iLDs and iTDs should ideally satisfy the following requirements,

1. For a significant frequency range, they should increase with the adjacency of the sound source and should reach their maximum at  $\theta = 90^\circ$  and their minimum at  $\theta = -90^\circ$ .
2. The iTD in particular should remain more or less constant for a given frequency range thereby mirroring the behaviour of the ITD. As different sets of neurons are sensitive to different frequencies, a constant delay is advantageous from the point of view of neuronal processing (cf. Sec. 1.2). This is equivalent to the requirement that the phase difference is directly proportional to the frequency (see (3.6)).
3. They should go to zero at  $\theta = 0^\circ$  and  $\theta = \pm 180^\circ$  meaning they should vanish when the object is directly in front of and behind the animal.

The last of these requirements is ensured by the symmetry of our system as  $p_0 = p_L$  at  $\theta = 0^\circ$  and  $\pm 180^\circ$ . The first and second, on the other hand are more subtle aren't necessarily satisfied for all systems but as we will subsequently see, with our choice of parameters they will be to a great degree.

### Internal Level Differences

In Fig. 3.7 (house gecko) and Fig. 3.8, we plot the variation of the iLD with direction and frequency. The conventions for the  $x$ - and  $y$ -axes remain the same as the ones in Figures 3.1 and 3.2. The iLDs vary systematically with frequencies and peaks at around 3 kHz for

the house gecko and around 1 kHz for the Tokay gecko. As expected, they are positive for ipsilateral directions and negative for contralateral. The contour plots serve the purpose of giving us the simultaneous frequency and direction dependence of the iLDs well but the satisfaction of requirement 1 given in the above list isn't automatically clear.

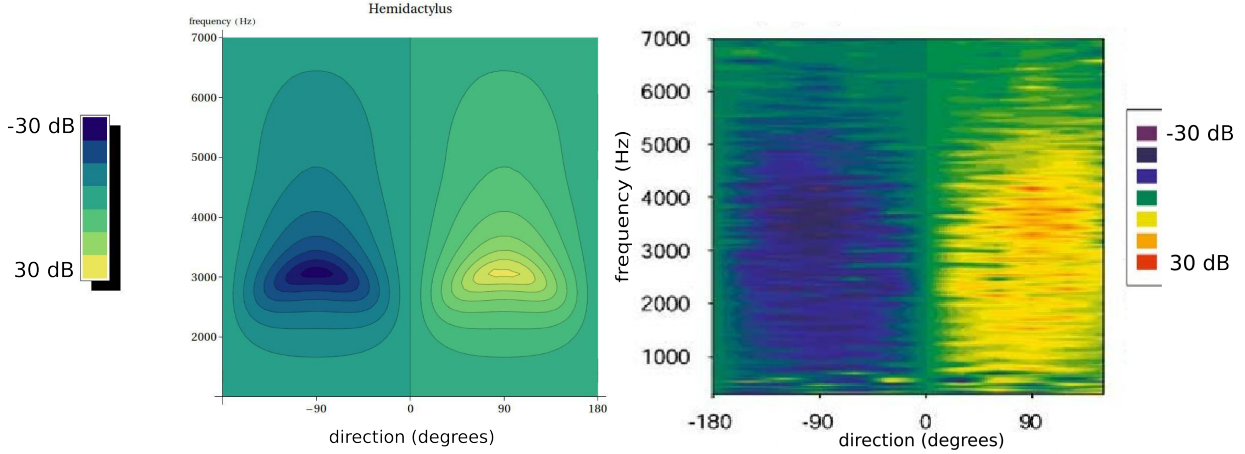


*Figure 3.7: Calculated (left) and experimental (right) Internal Level Differences (dB) of tympanic membrane vibrations for the common house gecko in dB. x-axis denotes direction in degrees (negative angles contralateral, 0 frontal and positive angles ipsilateral and the y-axis frequency in kHz. Calculated and experimental values [21] show similar qualitative behaviour. See also Fig. 3.8.*

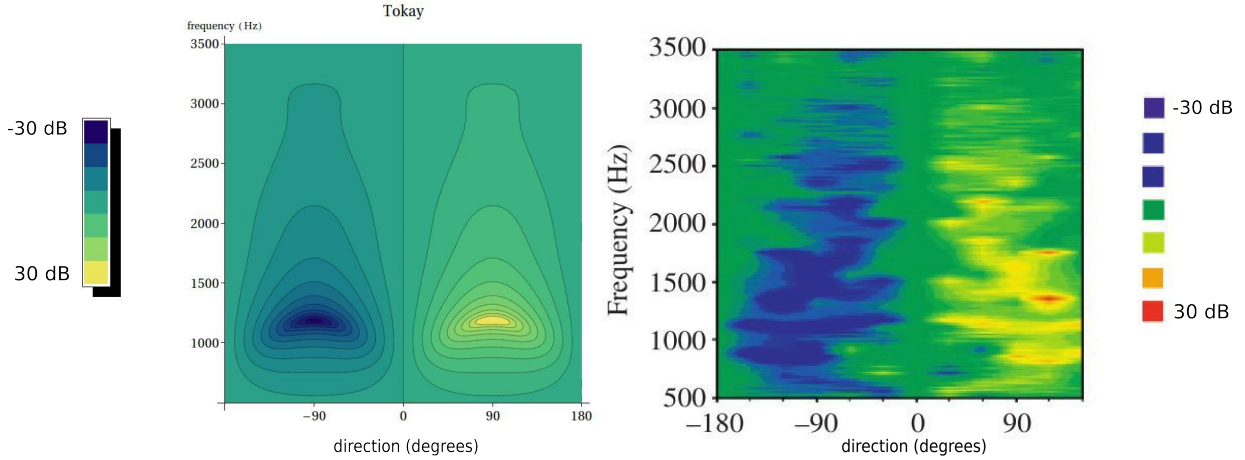


*Figure 3.8: Calculated (left) and experimental (right) Internal Level Difference of tympanic membrane vibrations for the Tokay gecko in dB. The experimental values are taken from Christensen-Dalsgaard [4].*

In order to better understand the direction dependence of iLD, we plot the variation of iLDs with direction for a given set of frequencies in Fig. 3.9 (left:the house gecko, right:and

Tokay gecko). We see that although the iLD has higher values below 3 kHz for the house gecko (below 1 kHz for the Tokay gecko), the form of the iLD for higher frequencies reflects the sinusoidal input better by peaking at fully ipsilateral and contralateral directions. This suggests that iLDs may work better as directional cues at higher frequencies. In Fig. 3.10 we see this behaviour more clearly. Here we have plotted the iLD for a stimulus at  $090^\circ$  with respect to frequency for both species. The bandpass behaviour is clearly shown - the house gecko has a maximum difference of 30 dB at around 3 kHz and the Tokay gecko iLD peaks at 36 dB at around 1 kHz. Also indicated in the figure is the directional bandwidth for both animals. This is defined as the frequency range in which the iLD for an ipsilateral stimulus differs by more than 3 dB. For the house gecko this is around 4.9 kHz and for the Tokay gecko it is around 2.6 kHz which is in very good agreement with experimentally observed values ([4], [21]). The fact that the calculated iLDs agree well with experimental values numerically suggests that the total membrane displacements are good measures of the membrane properties.

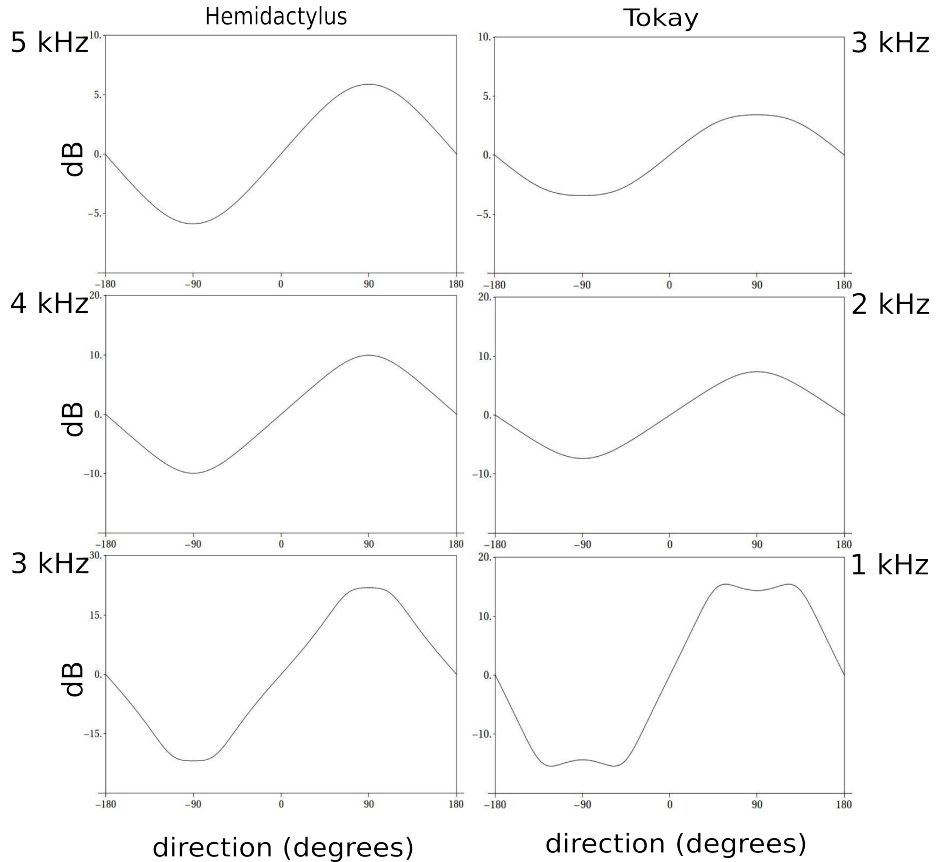


*Figure 3.9: Direction dependence of the Internal Level Difference (dB, cf. (3.5)) in the ICE Model for different frequencies - common house gecko (left, at 3kHz, 4kHz and 5kHz), Tokay gecko (right, at 1kHz, 2kHz and 3kHz). At higher frequencies, the iLD reaches a maximum at  $90^\circ$  and a minimum at  $-90^\circ$  whereas for lower frequencies, the maxima and minima are reached before and after. This form of the above plots suggests that the iLDs cannot by themselves be used to localize sources in this regime and work better as directional cues at relatively higher frequencies.*

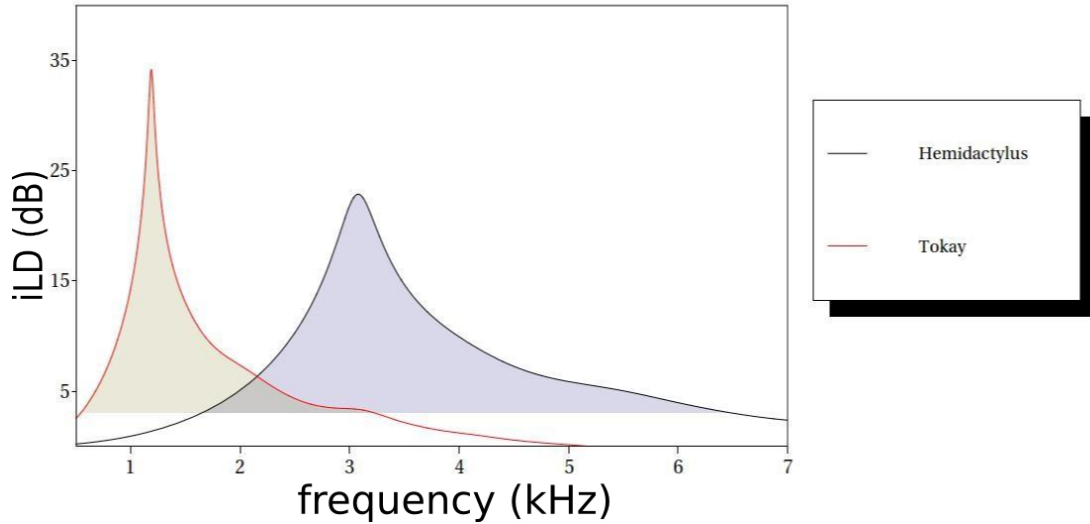


*Figure 3.10: Spectral behaviour of the iLDs at  $\theta = 90^\circ$  for the house gecko (black) and Tokay gecko (red). On the x-axis we have frequency in kHz and on the y-axis the iLD in decibels. The bandpass nature of the iLDs is clearly shown with a peaks at around 3 kHz for the house gecko and around 1 kHz for the Tokay gecko and is consistent with observations;[4], [21]. The filled regions correspond to the directional bandwidth (frequencies at which  $iLD > 3\text{dB}$ ) of both animals. This value is around 4.9 kHz for the house gecko and 2.6 kHz for the Tokay gecko.*

### Internal Time Differences

As we have just seen, the iLDs can be used as directional cues at relatively higher frequencies. The hearing range of geckos on the other hand is found to contain lower frequencies as well. In Fig. 3.11 we plot the variation of the iTD ( $\mu\text{s}$ ; cf. (3.6)) for a fully contralateral ( $-90^\circ$ ) stimulus for both species with respect to frequency. From the figures we see that requirement 2 is satisfied fairly well for both animals, albeit for different frequency ranges. At first, the lowpass behaviour as evidenced from the figure might seem counterintuitive as the input phase differences vanish at zero frequency. But as the phase difference between the membranes increases more or less linearly for low frequencies, a division by the angular frequency results in a constant value.

For the case of the house gecko, the iTD is around  $43.7 \mu\text{s}$  and the resultant iTD between 500 Hz and 2.7 kHz has an iTD gain (the ratio of the iTD w.r.t to the ITD) of around three (or an iTD of around  $123 \mu\text{s}$ ). For the Tokay gecko, the iTD is around  $96.2 \mu\text{s}$  which results in an iTD gain of around 3.6 (iTD of around  $346 \mu\text{s}$ ). These values stay more or less constant up to a certain frequency (around the first eigenfrequency of the membrane) and sharply drop. As the frequency increases beyond this point, the iTD converges to the ITD. In Fig. 3.12, we plot the variation of the iTDs with respect to direction for different frequencies. The frequencies are chosen to reflect the change in behaviour of the iTDs as it transitions from frequencies below the first eigenfrequencies to those above. At frequencies below the first eigenfrequency (Tokay: .5 kHz, 1 kHz, Hemidactylus: 1 kHz, 2 kHz) the

iTDs is significantly higher than it is at higher frequencies. At this point we should note that phase difference ceases to be useful as a directional cue when it is greater than  $2\pi$  or in other words when the iTD becomes greater than the time period at the given sound frequency ( $1/f$ ). Thankfully, for the frequency ranges we are concerned with this will not be a problem.

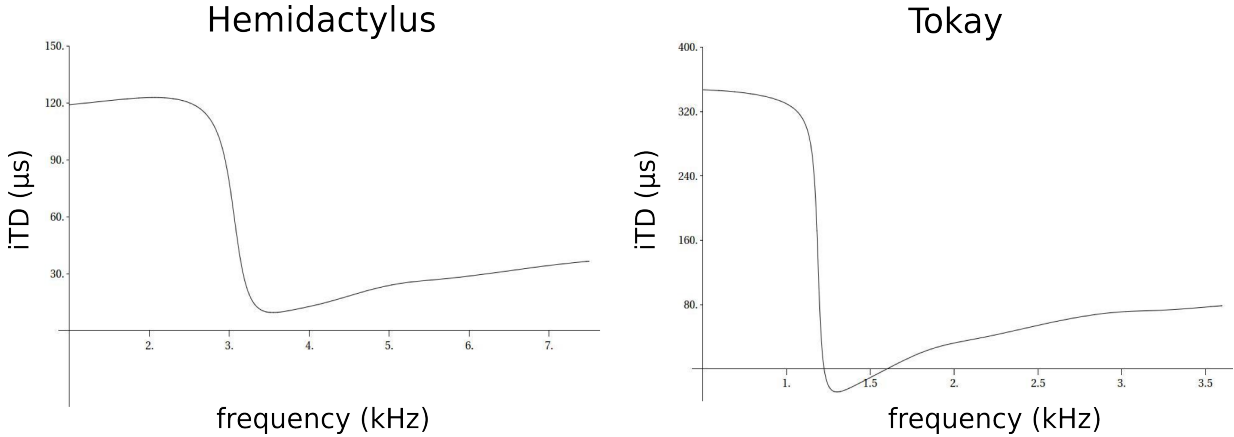


*Figure 3.11:* Spectral behaviour of the iTDs at  $\theta = 90^\circ$  for the house gecko (black) and Tokay gecko (red). On the x-axis we have frequency in kHz and on the y-axis the iTD in  $\mu\text{s}$ . The bandpass nature of the iTDs is clearly shown with a peaks at around 3 kHz for the house gecko and around 1 kHz for the Tokay gecko as is consistent with observations;[4], [21]. At frequencies above  $f_0$  there is a sharp drop and iTD cues are no better than ILD cues. At these frequencies however, the iTDs are high enough to be used as directional cues.

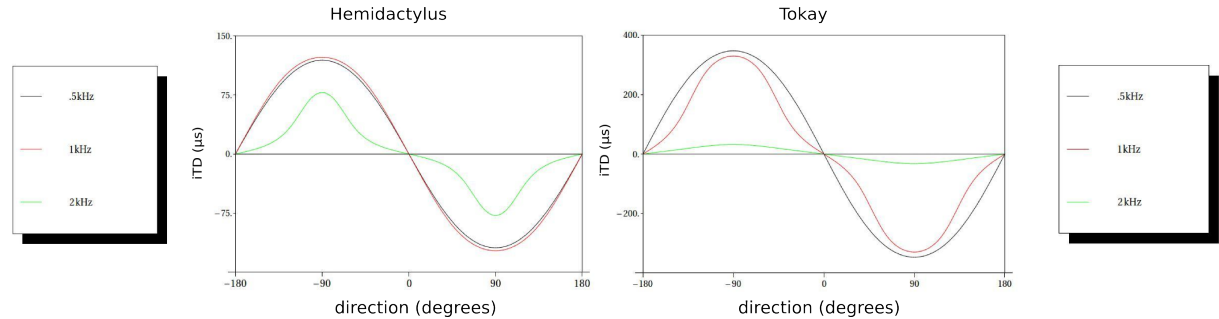


*Figure 3.12:* Variation of the iTD ( $\mu\text{s}$ ) with direction for different frequencies. We can clearly see that the iTD cues are more pronounced at frequencies below  $f_0$ .

The results up to this point tell us that just as in the case of animals with independent ears, animals with coupled ears may find it more efficient to use time difference cues (iTDS) at lower frequencies and level difference cues (iLDs) at higher frequencies. There might also be a frequency regime in which both cues can simultaneously be used. In humans

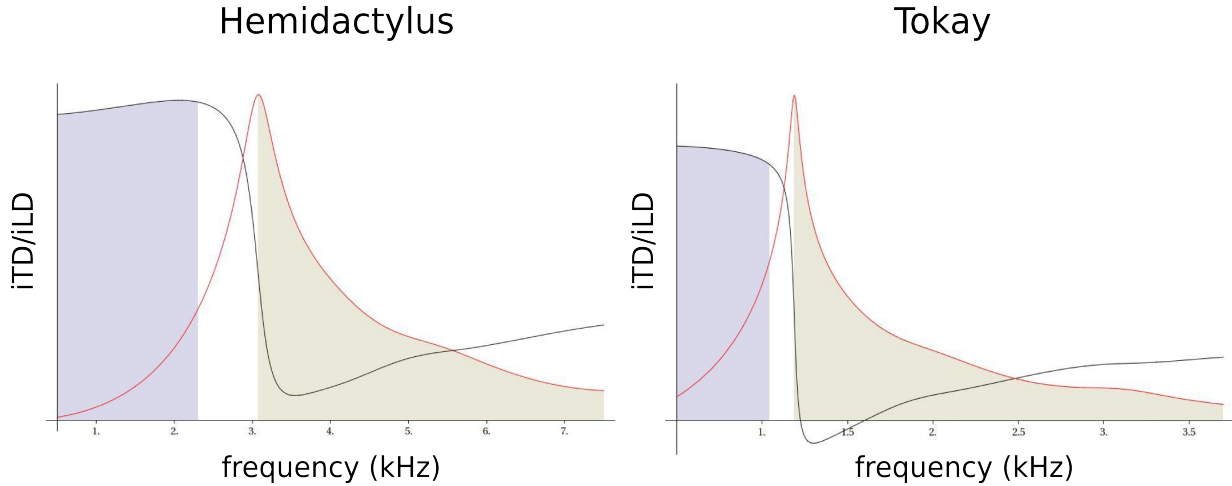


Figure 3.13: Possible regimes for the use of iTDs and iLDs for the house gecko (left) and Tokay gecko (right). The purple filled region corresponds to the iTD regime and the beige filled region to the iLD regime. There is also a possibility of an overlap region where both cues can be used. The iTD curves have been scaled to demonstrate the different regions more clearly. Ref. figures 3.10 and 3.11.

and other mammals these cues arise due to the diffraction of sound around the animals head and body resulting in inputs on both ears with measurable directional differences. Whereas in the ICE model, the only information about the direction of the sound source is in the form of a small phase difference between the inputs to both ears. these difference arise from the coupling between the ears and the cutoffs are determined by the system properties.

In Fig. 3.13 we simultaneously plot the iLD and iTD spectra in order to clearly demonstrate their regions of applicability. The iTD spectra have been scaled to have a similar height as the iLDs in order to clearly demarcate the regimes. The first region (purple) corresponds to the region where the iTD cues are more effective in ascertaining the direction of a sound source and the second region (beige) to the region where an iLD based localization is more effective. There is an additional possibility of an overlap region where both iTD and iLD cues can simultaneously be used.

### 3.1.3 Parameter Estimation

Up to this point we have calculated the desired quantities in our model by using the values given in Table 2.1. Some of the parameters can be directly taken from their measured values whereas the rest will need to be estimated indirectly. For the head width/interaural distance ( $L$ ), cavity volume ( $V_{\text{cav}}$ ), the density of the membrane ( $\rho_m$ )<sup>1</sup> and its thickness ( $d$ ) we can use the directly measured values. The radius of the cylinder ( $a_{\text{cyl}}$ ) can be calculated from the first two quantities using (2.1). As we've already seen in Fig. 2.5, the realistic

<sup>1</sup>A caveat: The density given in common models for the tympanum is around  $3 \text{ mg/mm}^3$  but this includes the mass of the transducer (the extracolumella). The density of the material of the tympanic membrane is in fact closer to the density of water, hence the chosen value of  $1 \text{ mg/mm}^3$

tympanic membrane is an ellipsoid rather than a perfect circle therefore the radius of our tympanum will instead be estimated from the area of the membrane as  $a_{\text{tym}} = \sqrt{A/\pi}$ . For the extracolumella angle ( $\beta$ ), we use the value estimated by Vossen [13].

The parameters that require an indirect estimation are the first membrane eigenfrequency ( $f_0$ ) and its quality factor  $Q$ . The first of these effectively gives us the propagation speed of membrane vibrations,  $c_M = 2\pi f_0 / \mu_{01}$  and the second gives us the membrane damping,  $\alpha = \pi f_0 / Q$ . These quantities are difficult to directly measure and instead have to be estimated from the frequency response of the system. In simulations of the ICE model, these parameters have been determined heuristically while keeping the requirements 1, 2 and 3 from page 42 in mind. Nevertheless, for future work it would be expedient to have a method to provide a rough estimate of these quantities from experimental results. In this way the calculation of relevant parameters gives us an idea of their typical values for a given species.

A hint for their approximate values comes from the bandpass nature of the Internal Level Differences and the frequency at which the iLD maximum is attained. This suggests that one of the membrane eigenmodes is dominant. In addition, as we have already seen, the iTDs remain constant for a significant frequency range ([15, p .1996]) putting further constraints on the value of  $Q$ . For the house gecko they have been experimentally is around 3 kHz and around 1.4 kHz for the Tokay gecko. Due to the complexity of the expression for the membrane vibration profile, the exact position of the iLD maximum is hard to directly calculate.

In order to better understand our parameter selection, we need to take a closer look at the analytical expression for the displacement ratio of the membranes and simplify the expression after using the appropriate formulas for  $G_{\text{ipsi}}^s$  and  $G_{\text{contra}}^s$ ,

$$\frac{\dot{S}^0}{\dot{S}^L} = \frac{\eta + e^{1.5jkL}}{1 + \eta e^{1.5jkL}} \quad (3.8)$$

where,  $\eta = \frac{G_{\text{ipsi}}^s}{G_{\text{contra}}^s} = \frac{\Lambda}{\rho c \omega} \sin kL - \cos kL$ .

We have also set the direction of the source to be fully ipsilateral to the  $x = 0$  membrane, i.e.  $90^\circ$ . The complex frequency dependence of the above term is entirely contained in the term  $\eta$ .

As stated towards the end of Sec. 2.2.3, we have to choose an appropriate cutoff for the value of  $\Lambda$ . In general, this choice depends on the values of  $f_0$  and  $Q$  and therefore on the hearing range of the animal. It is further complicated by the fact that the corresponding zeros of the Bessel function  $J_\kappa$  are very closely spaced. In our simulations up to this point we have chosen an arbitrary cutoff of the first 30 modes. A way around this difficulty can be found from the observation that the shape of the iLD spectrum (see Fig. 3.10). It suggests that one of the membrane eigenmodes dominates in the expansion of  $\Lambda$ . For the purposes of an estimation we can therefore calculate  $\Lambda$  up to the first eigenmode i.e. the

(1, 1) mode (ref. Fig. 2.9 and (2.59)). This gives us,

$$\eta = G \tilde{\Omega}_{01} \frac{\sin kL}{kL} - \cos kL \quad (3.9)$$

where,  $G = \frac{V_{\text{cav}} \rho_m d}{\rho c^2 K_{01}}$ .

The term  $G$  contains all the information from the “fixed” parameters like cavity volume, membrane density, thickness etc. and  $\tilde{\Omega}_{01} = (\omega^2 - 2j\alpha\omega - \omega_{01}^2)$  contains the as yet unknown parameters,  $f_0$  and  $Q$ . Substituting this expression in (3.8) gives us the displacement ratio as a function of the frequency. We now find expressions for the iTD and iLD in terms of the above ratio,

$$\text{iLD}_{90} = 10 \log_{10} \left( \frac{(\text{Re}(\eta) + \cos 1.5kL)^2 + (\text{Im}(\eta) + \sin 1.5kL)^2}{(\text{Re}(\eta) + \cos 1.5kL)^2 + (\text{Im}(\eta) - \sin 1.5kL)^2} \right) \quad (3.10)$$

$$\tan(\omega \times \text{iTD}_{90}) = \frac{(1 - |\eta|^2) \sin 1.5kL}{\text{Re}(\eta) + (1 + |\eta|^2) \cos 1.5kL} \quad (3.11)$$

using (3.5) and (3.6). We have used subscripts to indicate that the above terms have been calculated at  $\theta = 90^\circ$ . We essentially have an expression for the iLD and iTD spectra with two unknown parameters. We now need two equations for a given frequency (or a given pair of frequencies) that can be used to determine  $Q$  and  $f_0$ . The first of these equations is obtained by requiring that the derivative of the iLD goes to zero at a given frequency -  $f_{\max}$ , i.e. the experimentally determined frequency of peak amplitude difference.

The second equation requires us to put a constraint on the iTD. To do this we first look at the behaviour of the iTD for our system parameters for different values of  $Q$ . Qualitatively it can be said that the frequency of peak iLD is close to  $f_0$  with exact position depending on  $Q$  as well. The dependence of the iTD on  $Q$  is a little more complicated but perhaps more revealing. In Fig. 3.14, we plot the variation of the iTD spectrum for the three typical ranges of  $Q$ . At “low” values of  $Q$  the iTD increases up to a certain frequency and drops after reaching its maximum value,  $1/f_0$ . At higher values the iTD decreases steadily with frequency up to a certain value and somewhere in the middle, the iTD remains more or less constant up to a certain frequency. This behaviour gives evidence for the existence of an optimal value  $Q_0$  for which the iTD best satisfies requirement 2. Due to the relation of the iTD to the complex argument, we can approximate this requirement by requiring that the second derivative of the complex argument with respect to frequency vanishes at  $f_0$ .

These conditions can therefore be written as the following set of equations,

$$\left. \frac{d(\text{iLD}_{90})}{df} \right|_{f=f_{\max}} = 0 \quad (3.12)$$

$$\left. \frac{d^2 \omega(\text{iTD}_{90})}{df^2} \right|_{f=f_{\max}} = 0 \quad (3.13)$$

These give us a pair of nonlinear equations that can be numerically solved to obtain values for  $f_0$  and  $Q$ .

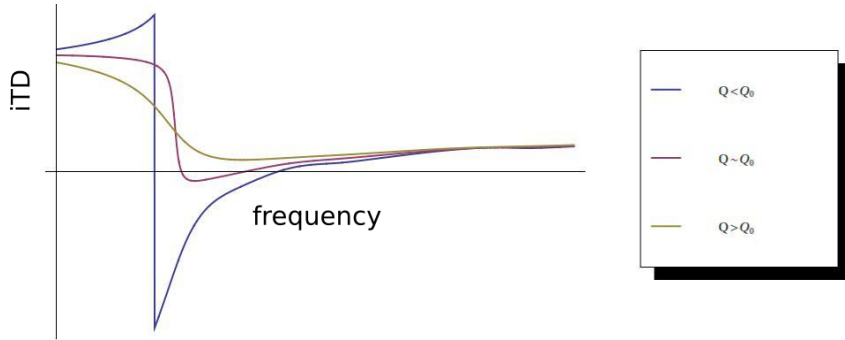


Figure 3.14: The three curves correspond to the iTD spectrum (cf. Fig. 3.11) for different values of  $Q$ . In the red curve we have the spectrum for a near ideal value of  $Q$  ( $Q_0$ ) such that the iTD remains more or less constant upto a given frequency. The blue curve corresponds to a low  $Q$  for which the iTD increases upto a peak value ( $1/f_0$ ) and drops afterwards. In the yellow curve we see that the iTD decreases steadily with frequency upto a certain point before converging to the ITD value.

## 3.2 Spatial Vibration Pattern of the Membrane

We begin our analysis by evaluating the variation of the spatial vibration pattern of the tympanic membrane with frequency. The tympanic vibration pattern was first measured experimentally by Manley [20] for a *Tokay gecko* and was found to have the strongest response at around 1kHz. The measured vibration patterns are shown on the left in Fig. 3.15. Manley measured the vibration amplitude for eight locations on the membrane and measured the pattern seen on the left of Fig. 3.15. As we can see, at around 4 kHz, the vibration pattern distinctly develops two maxima - something that would not happen to a centrally loaded tympanum except at frequencies well beyond the hearing range of geckos.

In order to compare our model with the experimental results, we plot the response of one of the membranes ( $x = 0$ , although  $x = L$  could be chosen equivalently due to the symmetry of the system) in our cylindrical ICE model calculated using (2.60). The opposite ear was chosen to be blocked, meaning  $p_L = 0$ . This is illustrated in Fig. 3.15 (right) for the same frequency range as in the experimental data. The sound pressure input was chosen to have unit amplitude and the model parameters used are given on the right most column of Table 3.1. The omitted region corresponds to the extracolumella.

The asymmetric nature of our membrane vibration pattern is a result of our chosen geometry. Mathematically this is a result of the fact that a uniform pressure (on the membrane surface) on a full circular membrane only couples to the circularly symmetric  $J_0$  modes. In the case of the sectoral membrane however, the uniform pressure couples to all the eigenmodes resulting in a more complex pattern. As a qualitative reproduction our model is very accurate but for a full quantitative analysis, we would need to account for the motion of the extracolumella. Moreover, the full mechanics of the extracolumella including its flection at higher frequencies can have significant effects which have not been studied so far.

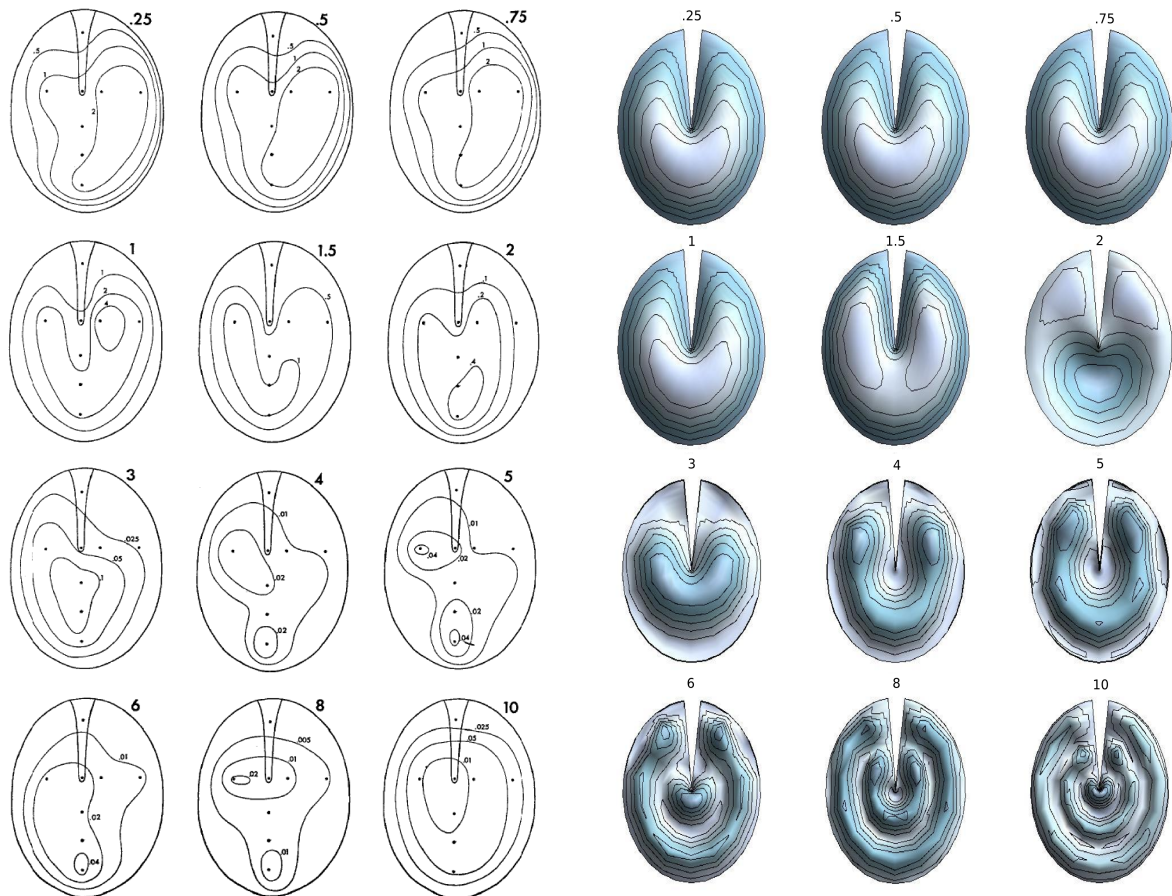


Figure 3.15: Left: Experimental membrane vibration patterns of the Tokay gecko dependent on sound frequency varying from .5 kHz to 10 kHz (corresponding frequency shown above membrane). Data taken from [20]. Right: Vibration pattern of one of the membranes in the ICE model with the opposite membrane blocked for the same frequency range. In both cases we see a similar complex vibrational pattern for the membranes which varies with frequency.



# Chapter 4

## Summary and Discussion

We started our study in Chapter 2 by constructing a basic model that describes the motion of eardrums in animals with coupled ears. The mouth cavity of the animal was modelled as an air-filled cylindrical tube of radius  $a_{\text{cyl}}$  with circular openings on either side of radius  $a_{\text{tymp}}$  that are closed by tympanic membranes of the same radius. This is one of the points where we deviate from the previous treatment of the problem [13] as we have kept the volume of the cavity  $V_{\text{cav}}$  constant and equal to typical values for the species in nature. The sound inputs to both ears took the form of pressure waves with a phase shift which depended on the frequency, direction of the source and head width and shape.

The second difference of our model from the previous treatment was the modelling of the membrane as a circular sector of angle  $2\pi - 2\beta$ . The remaining sector of angle  $2\beta$  represented the the extracolumella - the extension whose function is to serve as a transducer of membrane vibrations. We had modelled the extracolumella as being a stationary object and its effect on the membranes was given through additional boundary conditions at  $\phi = \pm\beta$ . The variation of air-pressure inside the tube was described by the 3D wave equation with no-penetration boundary conditions at the wall. In the previous treatment it was assumed that the pressure modes inside the cavity are identical to the circular modes on the membrane.

We then proceeded to find a solution to the full problem viz., the vibration of the membranes coupled through the cylindrical cavity. This required the application of a new set of boundary conditions at the membrane-air interface. These conditions were equivalent to the no-penetration boundary condition and required setting the membrane velocity to be equal to the velocity of air inside the cavity. The complexity of these boundary conditions required an approximation. We expanded the membrane velocity in terms of the pressure modes and used the zeroeth order of the expansion. Thus we effectively approximated the membrane by a piston oscillating with an amplitude equal to the integral of the membrane displacement. The approximation of the boundary condition simplified the expression of the pressure by approximating it as a plane wave propagating along the  $x$ -axis. In the frequency ranges of interest to us this turned out to be a reasonable assumption. At the end of the chapter we obtained expressions for the membrane displacements in terms of the input pressure inputs to both ears.

In Chapter 3 we evaluated the results of our model - specifically its direction and frequency. We started by comparing the total membrane displacements  $S^{0/L}$  (the integrals of the membrane displacement) with the experimentally measured values of displacement at the tip of the extracolumella. For the membrane velocities, we found that they vary systematically with direction and frequency and were in general higher in ipsilateral directions. The experimentally observed properties such as the marked asymmetry, steepness across the midline and general frequency response were also reproduced. The shape of the membrane velocities suggested that monoaural computation of membrane velocities would not serve well as directional cues.

We then went on to introduce the main directional cues in terms of the ratio  $S^0$  and  $S^L$ . Namely, the Internal Level Difference (iLD) which was defined as the decibel of the absolute value of this ratio and the Internal Time Difference (iTID) defined as its complex argument divided by the angular frequency  $\omega$ . In order to stress on the universality of the model, the calculated values of these quantities were compared with experimentally measured ones for two gekkonids - the common house gecko. (*Hemidactylus frenatus*) and the Tokay gecko (*Gekko gecko*). The simultaneous frequency and direction dependence of the iLD was illustrated by means of contour plots and were found to be consistent with experimental measurements - both in terms of qualitative spectral behaviour and quantitative values thus justifying our choice of  $S^{0/L}$  as measures of membrane displacement. We then introduced the requirements these cues must fulfil in order to effectively serve as directional cues. For the iLDs it was found that these requirements are best satisfied at relatively higher frequencies while iTIDs seem to be more effective at lower frequencies.

The model thus inherently contains frequency regimes for both directional cues. While in the case of mammals the use of ITD/ILD is dictated by the size of the head in comparison to the wavelength, the transition in the ICE model is dictated by the membrane properties like the fundamental eigenfrequency and damping. Certain parameters of the model were directly based on experimental values - membrane density, radius and thickness, cavity volume, head width etc. The other membrane specific parameters such as its first eigenfrequency and its damping coefficient are hard to experimentally determine. In Sec. 3.1.3 we therefore presented a possible method to estimate these parameters from observations. We ended the chapter by illustrating the vibrations patterns of one of the ICE-model membranes with the opposite one blocked. These patterns were compared and found to be in good agreement with the patterns experimentally measured for the Tokay gecko by Manley [20].

## 4.1 Biological Relevance

In this thesis we have presented a general model for ears coupled through a large air cavity. Although we have restricted the comparison of our results with membrane vibration data for gekkonids from Dalsgaard and Manley ([4],[21]) and Dalsgaard *et al* [15], our model readily describes the coupling between eardrums across a range of gekkonid species by substituting the appropriate parameters for cavity volume ( $V_{\text{cav}}$ ), head width, tympanum

area etc. The model can also be adapted to other animals with ICE such as birds and the main modification to be made would be to the transducer (the extracolumella in our case). For example, the extracolumella in birds is generally centrally attached to the eardrum [34] resulting in a different set of membrane eigenmodes.

The agreement of our calculations with experimental results suggests that the exact shape of the cavity does not have an effect as significant as  $V_{\text{cav}}$  on the hearing cues. The previously unaccounted for effect of diffraction on the input phase difference was also seen to have a significant effect on both the iTDs and iLDs. The ICE model also places natural limits on iTD and iLD based hearing dependent on the fundamental membrane eigenfrequency. As we have seen in Sec. 3.1.2, the transition frequency from iTD based localization to iLD based localization is close to the membrane eigenfrequency. For this reason it isn't unreasonable to expect that animals with typically higher hearing ranges will tend to have higher membrane eigenfrequencies and vice versa. In contrast with mammals, in whom this transition is determined by their size, the transition between the two regimes is entirely a consequence of the physics of the ICE model.

By using a cylindrical air cavity as opposed to a circuit model for the coupled system (Zhang *et al* [32]), we have been able to account for the high frequency behaviour of the system which is a result of significant pressure amplitude differences between the ears. This also leads to the additional possibility of using the ICE model to explain hearing in animals such as crocodilia. As shown by Vergne *et al* [35] and Higgs *et al* [36] they seem to be able to hear well both above and underwater while using the same neural processing pathways for both environments. The speed of sound in water is four times that in air and as a result wavelengths for the same frequency are quadrupled as well. There is a possibility of switching to an ICE like system to overcome this problem when underwater.

## 4.2 Open Questions

The main advantage of the ICE-model is to explain the frequency and direction dependence of the hearing cues. In order to have a complete quantitative description of the ICE-model, we would also need to take into account the motion of the extracolumella and the exact shape of realistic mouth cavities. The first of these can be treated analytically up to a point. The main modification would be in the membrane boundary conditions corresponding to the extracolumella. Instead of setting the displacement to zero, we would need to take into account the mass of the extracolumella resulting in a new equation of motion. This equation would describe the motion of the extracolumella driven by the membrane tension and the internal and external pressure difference. A further step would be to incorporate the flexion of the extracolumella at higher frequencies as described by Manley [20]. This would require a further understanding of its constituent cartilaginous material and would necessitate a numerical treatment.

Due the complex shape of a realistic mouth cavity, a full treatment is not conducive to an analytical treatment. Numerical software like COMSOL can be used to treat reconstructions of mouth casts. Another possibility would be to include the effect of the nostrils

as either a new set of boundary conditions or a third input source. The eigenfrequencies of the mouth cavity were studied by Vossen [14, p. 39] but the influence of the holes corresponding to the membranes was neglected here. Additionally, the neuronal basis of the computation of iTD cues is not fully understood and the applicability of the Jeffress model in their case has also been called into question. Lastly, the response of the animal to sound stimuli in realistic environments viz. in the presence of multiple obstacles could also be a topic for further study. This however necessitates further experimental analyses of sound localization in vertebrates.

# Appendix A

## Mathematica Code

The Mathematica code used to calculate the total membrane displacements, iTD and iLD. The original input values are for the Tokay gecko. The corresponding parameters for the house gecko are given in the comments.

```
Speciesname = "Hemidactylus"; "or Tokay";  
L:=10; "Cylinder Length in mm. 10/22";  
atymp:=1.5; "Radius of Tympanic Membrane in mm. 1.5/2.6";  
ρm = 1; "1.25*.3125;" "Density of Membrane in mg/mm^3";  
d = .008; "Membrane Thickness in mm. .008/.01";  
β:=Pi/25; "Extracollumella angle";  
μ = Pi/(Pi - β);  
(*cM = 25000; *)  
(*ρ = 1.162 * 10^-3; "Density of Air mg/mm^3"; *)  
V0 = 320; "320/3500, mm^3";  
acyl = Sqrt[V0/(Pi * L)];  
"Volume of the Cylinder";  
γ = 1.4; "Ratio of Specific Heats for Air";  
P0 = 101.325 * 10^6; "Atmospheric Pressure";  
(*c:=Sqrt[γ * P0/ρ]; "Velocity of Sound mm/s"; *)  
c = 343000;  
ρ = γ * P0/c^2; "Density of Air mg/mm^3";
```

```
f0 = 2800; "2800/1050";
 $\alpha = .75 * 2 * \text{Pi} * f0/2.4;$  "Damping Coefficient of Membrane in Hz";
"Sound inputs to both ears";
 $\Phi = \text{Pi} * \text{TriangleWave}[\theta/360]/2;$ 
 $\omega = 2 * \text{Pi} * f;$ 
```

$k = \omega/c;$

```
p0 = 1000 * E^(-.75 * I * k * L * (Sin[\thetaDegree])); "Pressure is 1Pa in units of mg/(mm s^2)";
pL = 1000 * E^(.75 * I * k * L * (Sin[\thetaDegree]));
```

"Calculating and sorting the zeros of the membrane modes Bessel Functions";

```
allZeros = Sort[Flatten[Table[{(l + .5) * \mu, m, BesselJZero[(l + .5) * \mu, m]/atyp}, {l, 0, 9}, {m, 1, 6}], 1],
{#1[[3]] < #2[[3]]] &];
```

"Membrane Propagation Velocity in terms of the first eigenfrequency mm/s";

```
cM = f0 * 2 * Pi/allZeros[[1]][[3]];
```

Ncutoff = 30; "Cutoff for the membrane modes";

"Membrane impulse response";

$\Lambda =$

```
(Sum[Integrate[r * Sin[allZeros[[l]][[1]] * (\phi - \beta)] * BesselJ[allZeros[[l]][[1]], allZeros[[l]][[3]] * r],
{r, 0, atyp}, {\phi, \beta, 2 * Pi - \beta}]^2 /
(\rho_m * d * (\omega^2 - 2 * I * \alpha * \omega - cM^2 * allZeros[[l]][[3]]^2) *
Integrate[r * Sin[allZeros[[l]][[1]] * (\phi - \beta)]^2 *
BesselJ[allZeros[[l]][[1]], allZeros[[l]][[3]] * r]^2, {r, 0, atyp}, {\phi, \beta, 2 * Pi - \beta}]),
{l, 1, Ncutoff}])^2 - 1;
```

"Calculation of the total membrane displacements";

```
Gamplus = -\rho * \omega^2 * Cot[k * L/2]/(Pi * acyl * acyl * k);
```

```
Gamminus = \rho * \omega^2 * Tan[k * L/2]/(Pi * acyl * acyl * k);
```

```
Splus = (pL + p0)/(Gamplus + \Lambda);
```

---

```

Sminus = (pL - p0)/(Gamminus + Λ);
SL = (Splus - Sminus)/2;
S0 = (Splus + Sminus)/2;

“Internal Level Difference”;
iLD = 20 * Log10[Abs[S0/SL]];
“Internal Time Difference”;
iTД = Arg[S0/SL]/ω;

Needs[“PlotLegends”];

“Plot ticks for direction and frequency”;
dticks = Table[{(l - 1) * 90 - 180, ToString[(l - 1) * 90 - 180], {0, .01}}, {l, 1, 5}];
fticks = Table[{l * fmin, ToString[l * fmin], {0, .01}}, {l, 1, 7}];

“Density Plot of Membrane Vibration Amplitude”;
ShowLegend[ DensityPlot[20 * Log10[ω * Abs[S0]/(Pi * acyl * acyl)], {θ, -180, 180}, {f, fmin, fmax},
ColorFunction → “BlueGreenYellow”, PlotPoints → 20, Frame → False, Axes → True,
AxesOrigin → {-180, 200}, AxesLabel → {None, “frequency (Hz)”), Ticks → {dticks, fticks},
PlotLabel → Speciesname, FrameLabel → {“direction(degrees)”, None}],
{ColorData[“BlueGreenYellow”][#1]&, 8, “-30”, “10”, LegendPosition → {-1.5, -.35},
LegendOrientation → Vertical}]

“Membrane vibration spectrum for different source directions”;
dbticks = Table[{(l - 1) * 10 - 40, ToString[(l - 1) * 10 - 40], {0, .005}}, {l, 1, 6}];
fticks = Table[{l * fmin, ToString[N[l * fmin/1000]], {0, .01}}, {l, 1, 7}];

Plot[{20 * Log10[ω * Abs[S0]/(Pi * acyl * acyl)]/.θ → 90, 20 * Log10[ω * Abs[S0]/(Pi * acyl * acyl)]/.θ → 60,
20 * Log10[ω * Abs[S0]/(Pi * acyl * acyl)]/.θ → 0, 20 * Log10[ω * Abs[S0]/(Pi * acyl * acyl)]/.θ → -60,
20 * Log10[ω * Abs[S0]/(Pi * acyl * acyl)]/.θ → -90}, {f, fmin, fmax}, PlotRange → {-40, 10},
PlotStyle → {ColorData[1][1], ColorData[1][2], Dotted, Dashed, Dashed}, AxesOrigin → {500, -40},
Style[Speciesname, 16], Epilog → {Line[{{5000, -40}, {5000, 10}, {500, 10}, {5000, 10}}]}];

```

```
Ticks → {fticks, dbticks}, PlotLegend → {"90°", "60°", "0°", "-60°", "-90°"}, LegendPosition → {.9, -.4}]
```

"Membrane vibration direction dependence";

ftest = 1000; "Test Frequency - refer Chapter 3 for values";

```
mrangle = Floor[-10 + 20 * Log10[ω * Abs[S0]/(Pi * acyl * acyl)]/.{f → ftest, θ → -90}];
```

```
prange = Ceiling[10 + 20 * Log10[ω * Abs[S0]/(Pi * acyl * acyl)]/.{f → ftest, θ → 90}];
```

```
ndbticks = 5;
```

```
dbticks =
```

```
Table[{(l - 1) * (prange - mrangle)/(ndbticks - 1) + mrangle,
```

```
ToString[N[(l - 1) * (prange - mrangle)/(ndbticks - 1) + mrangle]], {0, .005}], {l, 1, ndbticks}];
```

```
Plot[20 * Log10[ω * Abs[S0]/(Pi * acyl * acyl)]/.f → ftest, {θ, -180, 180}, PlotRange → {mrangle, prange},
```

```
PlotStyle → Black, AxesOrigin → {-180, mrangle}, PlotLabel → ToString[ftest] <> "Hz",
```

```
Ticks → {dticks, dbticks}, Epilog → {Line[{{180, mrangle}, {180, prange}, {-180, prange}, {180, prange}}]}]
```

"iLD with respect to direction and frequency";

```
range = 15 + 20 * Log10[Abs[S0/SL]]/.{f → f0, θ → 90};
```

```
ShowLegend[ContourPlot[20 * Log10[Abs[S0/SL]], {θ, -180, 180}, {f, fmin, fmax},
```

```
ColorFunction → "BlueGreenYellow", PlotPoints → 20, Contours → 20, Frame → False, Axes → True,
```

```
PlotRange → range, AxesOrigin → {-180, 200}, AxesLabel → {None, "frequency (Hz)"},
```

```
Ticks → {dticks, fticks}, PlotLabel → Speciesname, FrameLabel → {"direction(degrees)", None}],
```

```
{ColorData["BlueGreenYellow"][[#1]&, 8, "-30", "10", LegendPosition → {-1.5, -.35},
```

```
LegendOrientation → Vertical}]
```

"iLD direction dependence";

ftest = 1000; "Test Frequency - refer Chapter 3 for values";

```
mrangle = Floor[-10 + 20 * Log10[Abs[S0/SL]]/.{f → ftest, θ → -90}];
```

```
prange = Ceiling[10 + 20 * Log10[Abs[S0/SL]]/.{f → ftest, θ → 90}];
```

```
ndbticks = 5;
```

---

```

dbticks = 

Table[{(l - 1) * (prange - mrange)/(ndbticks - 1) + mrange,
ToString[N[(l - 1) * (prange - mrange)/(ndbticks - 1) + mrange]], {0, .005}}, {l, 1, ndbticks}];

Plot[20 * Log10[Abs[S0/SL]]/.f → ftest, {θ, -180, 180}, PlotRange → {mrange, prange},
PlotStyle → Black, AxesOrigin → {-180, mrange}, PlotLabel → ToString[ftest] <> "Hz",
Ticks → {dticks, dbticks}, Epilog → {Line[{{180, mrange}, {180, prange}, {-180, prange}, {180, prange}}]}]

"iLD spectrum with directional bandwidth";

ndbticks = 5;

dbticks = Table[{(l - 1) * 40/(ndbticks - 1), ToString[N[(l - 1) * 40/(ndbticks - 1)]], {0, .005}},
{l, 1, ndbticks}];

Plot[{20 * Log10[Abs[S0/SL]]/.{θ → 90}, If[(20 * Log10[Abs[S0/SL]]/.{θ → 90}) > 3, 3]},
{f, fmin, fmax}, PlotRange → {0, 40}, PlotStyle → {Black, None}, Ticks → {fticks, dbticks, None, None},
AxesOrigin → {fmin, 0}, Filling → {1 → {2}}, Epilog → {Line[{{fmin, 40}, {fmax, 40}, {fmax, 0}, {fmax, 40}}]}]

"iT D spectrum";

Tmax = Round[6 * L * 10^6/c, 50];

nticks = 6;

tticks = Table[{(l - 1) * Tmax/(nticks - 1), ToString[N[(l - 1) * Tmax/(nticks - 1)]], {0, .005}},
{l, 1, ntticks}];

Plot[{10^6 * Arg[S0/SL]/ω/.θ → 90}, {f, fmin, fmax}, PlotRange → {-40, Tmax}, AxesOrigin → {fmin, 0},
Ticks → {fticks, tticks}, PlotRange → All, PlotStyle → Black]

"iT D direction dependence";

ftest1 = 1000;

nticks = 9;

tticks = Table[{-Tmax + 2 * (l - 1) * Tmax/(nticks - 1), ToString[N[-Tmax + 2 * (l - 1) * Tmax/(nticks - 1)]],
{0, .005}}, {l, 1, ntticks}];

Plot[{10^6 * Arg[SL/S0]/ω/.f → ftest1, 10^6 * Arg[SL/S0]/ω/.f → 2 * ftest1,

```

---

```

10^6 * Arg[SL/S0]/ω/.f → 3 * ftest1}, {θ, -180, 180}, PlotRange → Tmax, PlotStyle → {Black, Red, Green},
AxesOrigin → {-180, -Tmax}, Ticks → {dticks, tticks},
Epilog → {Line[{ {-180, 0}, {180, 0}, {180, -Tmax}, {180, Tmax}, {-180, Tmax}, {180, Tmax} }]},
PlotLegend → {Style["1kHz", Black, 18], Style["2kHz", Black, 18], Style["3kHz", Black, 18]},
LegendPosition → {-2.0, -25}]

```

"Membrane Vibration Profile";

membamp =

```

Sum[Integrate[r * Sin[allZeros[[l]][[1]] * (ϕ - β)] * BesselJ[allZeros[[l]][[1]], allZeros[[l]][[3]] * r],
{r, 0, atymp}, {ϕ, β, 2 * Pi - β}] * Sin[allZeros[[l]][[1]] * (ϕ - β)] *
BesselJ[allZeros[[l]][[1]], allZeros[[l]][[3]] * r]/
(ρm * d * (ω^2 - 2 * I * α * ω - cM^2 * allZeros[[l]][[3]]^2) *
Integrate[r * Sin[allZeros[[l]][[1]] * (ϕ - β)]^2 *
BesselJ[allZeros[[l]][[1]], allZeros[[l]][[3]] * r]^2, {r, 0, atymp}, {ϕ, β, 2 * Pi - β}]),
{l, 1, Ncutoff}];
ipsimemb = Λ * membamp * (1/(Gamplus + Λ) + 1/(Gamminus + Λ));
flist = {250, 500, 750, 1000, 1500, 2000, 3000, 4000, 5000, 6000, 8000, 10000};
ftest = flist[[1]];
membplot = Re[ipsimemb/.f → ftest];
RevolutionPlot3D[membplot, {r, 0, atymp}, {ϕ, β, 2 * Pi - β},
ColorFunction → Function[{x, y, z, t, θ, r}, ColorData["Aquamarine"][z]],
MeshFunctions → {Function[{x, y, z, t, θ, r}, Evaluate[z]]}, MeshStyle → Thick, Mesh → 8,
Boxed → False, Axes → False, PlotLabel → Style[ToString[N[ftest/1000]], 24]]

```

# Bibliography

- [1] C. E. Carr, D. Soares, J. Smolders, and J. Z. Simon, “Detection of interaural time differences in the alligator,” *J. Neurosci.*, vol. 29, pp. 7978–7990, Jun 2009.
- [2] J. Christensen-Dalsgaard and C. Carr, “Evolution of a sensory novelty: tympanic ears and the associated neural processing.,” *Brain Res Bull*, vol. 75, no. 2-4, pp. 365–70, 2008.
- [3] J. W. Schnupp and C. E. Carr, “On hearing with more than one ear: lessons from evolution,” *Nature Neuroscience*, vol. 12, pp. 692–697, jun 2009.
- [4] J. Christensen-Dalsgaard and G. A. Manley, “Directionality of the lizard ear,” *J. Exp. Biol.*, vol. 208, pp. 1209–1217, Mar 2005.
- [5] A. Michelsen, “Hearing and sound communication in small animals: Evolutionary adaptations to the laws of physics,” in *The Evolutionary Biology of Hearing* (D. Webster, A. Popper, and R. Fay, eds.), pp. 61–77, Springer New York, 1992.
- [6] H. Autrum, “Über lautäußerungen und schallwahrnehmung bei anthropoden ii.,” *Journal of Comparative Physiology*, vol. 28, pp. 326–352, 1940.
- [7] A. Michelsen and O. N. Larsen, “Pressure difference receiving ears,” *Bioinspiration & Biomimetics*, vol. 3, no. 1, p. 011001, 2008.
- [8] H. F. Olson, “Gradient microphones,” *The Journal of the Acoustical Society of America*, vol. 17, no. 3, pp. 192–198, 1946.
- [9] D. Robert, R. Miles, and R. Hoy, “Directional hearing by mechanical coupling in the parasitoid fly *ormia ochracea*,” *Journal of Comparative Physiology A*, vol. 179, no. 1, pp. 29–44, 1996.
- [10] A. Michelsen, “Biophysics of sound localization in insects,” in *Comparative Hearing: Insects* (R. Hoy, A. Popper, and R. Fay, eds.), vol. 10 of *Springer Handbook of Auditory Research*, pp. 18–62, Springer New York, 1998.
- [11] M. Jørgensen, “Comparative studies of the biophysics of directional hearing in anurans,” *Journal of Comparative Physiology A*, vol. 169, no. 5, pp. 591–598, 1991.

- [12] A. Michelsen and K. Rohrseitz, "Sound localisation in a habitat: An analytical approach to quantifying the degradation of directional cues," *Bioacoustics*, vol. 7, no. 4, pp. 291–313, 1997.
- [13] C. Voßen, J. Christensen-Dalsgaard, and J. L. van Hemmen, "Analytical model of internally coupled ears.," *Journal of the Acoustical Society of America*, vol. 128, pp. 909–918, 2010.
- [14] C. Voßen, *Auditory Information Processing in Systems with Internally Coupled Ears*. PhD thesis, Technische Universität München, 2010.
- [15] J. Christensen-Dalsgaard, Y. Tang, and C. E. Carr, "Binaural processing by the gecko auditory periphery," *J. Neurophysiol.*, vol. 105, pp. 1992–2004, May 2011.
- [16] L. A. Jeffress, "A place theory of sound localization," *Journal of Comparative and Physiological Psychology*, vol. 41, pp. 35–39, feb 1948.
- [17] C. E. Carr and M. Konishi, "Axonal delay lines for time measurement in the owl's brainstem," *Proc. Natl. Acad. Sci. U.S.A.*, vol. 85, pp. 8311–8315, Nov 1988.
- [18] T. N. Parks and E. W. Rubel, "Organization and development of brain stem auditory nuclei of the chicken: organization of projections from n. magnocellularis to n. laminaris," *J. Comp. Neurol.*, vol. 164, pp. 435–448, Dec 1975.
- [19] G. Manley, "Frequency response of the middle ear of geckos," *Journal of comparative physiology*, vol. 81, no. 3, pp. 251–258, 1972.
- [20] G. A. Manley, "The middle ear of the tokay gecko," *Journal of Comparative Physiology*, vol. 81, no. 3, pp. 239–250, 1972.
- [21] J. Christensen-Dalsgaard and G. Manley, "Acoustical coupling of lizard eardrums," *Journal of the Association for Research in Otolaryngology*, vol. 9, no. 4, pp. 407–416, 2008.
- [22] C. Köppl and C. Carr, "Maps of interaural time difference in the chickens brainstem nucleus laminaris," *Biological Cybernetics*, vol. 98, no. 6, pp. 541–559, 2008.
- [23] L. Rayleigh and A. Lodge, "On the acoustic shadow of a sphere. with an appendix, giving the values of legendre's functions from p0 to p20 at intervals of 5 degrees," *Philosophical Transactions of the Royal Society of London. Series A, Containing Papers of a Mathematical or Physical Character*, vol. 203, pp. pp. 87–110, 1904.
- [24] L. Rayleigh, *Theory of Sound: V. 1*. Dover Publications., 1900.
- [25] S. Rschevkin, O. Blunn, and P. Doak, *A Course OF Lectures On Sound*. Pergamon, 1963.

- [26] S. Temkin, *Elements of Acoustics*. Wiley, 1981.
- [27] E. T. Copson, *Introduction to the Theory of Functions of a Complex Variable*. Oxford: Clarendon Press, 1973.
- [28] C. Pozrikidis, *Fluid Dynamics: Theory, Computation, and Numerical Simulation*. Springer, 2009.
- [29] N. Asmar, *Partial Differential Equations with Fourier Series and Boundary Value Problems*. Pearson Education, Limited, 2005.
- [30] N. H. Fletcher, *Acoustic Systems in Biology*. Oxford: Oxford University Press, 1992.
- [31] C. Rajalingham, R. Bhat, and G. Xistris, “Vibration of circular membrane backed by cylindrical cavity,” *International Journal of Mechanical Sciences*, vol. 40, no. 8, pp. 723 – 734, 1998.
- [32] L. Zhang, J. Hallam, and J. Christensen-Dalsgaard, “Modelling the peripheral auditory system of lizards,” in *From Animals to Animats 9* (S. Nolfi, G. Baldassarre, R. Calabretta, J. Hallam, D. Marocco, J.-A. Meyer, O. Miglino, and D. Parisi, eds.), vol. 4095 of *Lecture Notes in Computer Science*, pp. 65–76, Springer Berlin Heidelberg, 2006.
- [33] M. Jørgensen, B. Schmitz, and J. Christensen-Dalsgaard, “Biophysics of directional hearing in the frog eleutherodactylus coqui,” *Journal of Comparative Physiology A*, vol. 168, no. 2, pp. 223–232, 1991.
- [34] R. Mills, “Applied comparative anatomy of the avian middle ear,” *J R Soc Med*, vol. 87, pp. 155–156, Mar 1994.
- [35] A. L. Vergne, M. B. Pritz, and N. Mathevon, “Acoustic communication in crocodilians: from behaviour to brain,” *Biological Reviews*, vol. 84, pp. 391–411, aug 2009.
- [36] D. M. Higgs, E. F. Brittan-Powell, D. Soares, M. J. Souza, C. E. Carr, R. J. Dooling, and A. N. Popper, “Amphibious auditory responses of the American alligator (*Alligator mississippiensis*),” *J. Comp. Physiol. A Neuroethol. Sens. Neural. Behav. Physiol.*, vol. 188, pp. 217–223, Apr 2002.